BIOMIMETIC SELF-ASSEMBLED PEPTIDE NANOFIBERS FOR BONE REGENERATION

A THESIS

SUBMITTED TO THE MATERIALS SCIENCE AND NANOTECHNOLOGY PROGRAM OF GRADUATE SCHOOL OF ENGINEERING AND SCIENCE OF BILKENT UNIVERSITY

IN PARTIAL FULFILLMENT OF THE REQUIREMENTS

FOR THE DEGREE OF

MASTER OF SCIENCE

By

Samet Kocabey

August 2012

I certify that I have read this thesis and that in my opinion it is fully adequate, in scope and in quality, as a thesis for the degree of Master of Science.

_____

Assist. Prof. Dr. Ayse Begum Tekinay (Advisor)

I certify that I have read this thesis and that in my opinion it is fully adequate, in scope and in quality, as a thesis for the degree of Master of Science.

_____

Assoc. Prof. Dr. Mustafa Ozgur Guler (Co-Advisor)

I certify that I have read this thesis and that in my opinion it is fully adequate, in scope and in quality, as a thesis for the degree of Master of Science.

_____

Assist. Prof. Dr. Turgay Tekinay

I certify that I have read this thesis and that in my opinion it is fully adequate, in scope and in quality, as a thesis for the degree of Master of Science.

_____

Assist. Prof. Dr. Fatih Buyukserin

Approved for the Graduate School of Engineering and Sciences:

_____

Prof. Dr. Levent Onural

Director of Graduate School of Engineering and Science

ABSTRACT

BIOMIMETIC SELF-ASSEMBLED PEPTIDE NANOFIBERS FOR BONE REGENERATION

Samet Kocabey

M.S. in Materials Science and Nanotechnology

Supervisor: Assist. Prof. Dr. Ayse Begum Tekinay (Advisor)

August 2012

Self-assembled peptide nanofibers are exploited in regenerative medicine applications due to their versatile, biofunctional and extracellular-matrix-resembling structures. These properties provide peptide nanofibers with osteoinductive and osteoconductive behaviors for bone regeneration applications through several approaches. In this thesis, two different approaches were discussed, which were developed to induce bone regeneration and mineralization including extracellular matrix mimicking peptide nanofibers based 2-D gel formation and surface functionalization of titanium implants. For this purpose, we designed glycosaminoglycan-mimetic peptide nanofibers inspired by chemical structure of glycosaminoglycans present in the bone extracellular matrix. We demonstrated that glycosaminoglycan-mimetic peptide nanofibers interact with BMP-2, a critical growth factor for osteogenic activity.

Glycosaminoglycan-mimicking ability of the peptide nanofibers and their interaction with BMP-2 promoted osteogenic activity of and mineralization by osteoblastic cells. ALP activity, Alizarin Red Staining and EDAX spectroscopy indicated efficacy of the peptide nanofibers for inducing mineralization.

We also developed a hybrid osteoconductive system for titanium biomedical implants inspired by mussel adhesion mechanism in order to overcome bone tissue integration problems. For this purpose, Dopa conjugated peptide nanofiber coating was used along with bioactive peptide sequences for osteogenic activity to enhance osseointegration of titanium surface. Dopa-mediated immobilization of osteogenic peptide nanofibers on titanium surfaces created an osteoconductive interface between osteoblast-like cells and inhibited adhesion and viability of soft tissue forming fibroblasts compared to the uncoated titanium substrate.

In summary, osteoinductive and osteoconductive self-assembled peptide nanofibers were developed to promote osteogenic activity and mineralization of osteogenic cells. These bioactive nanofibers provide a potent platform in clinical applications of bone tissue engineering.

Keywords: Peptide Nanofibers, Biomimetic, Self-Assembly, Extracellular Matrix, Glycosaminoglycans, Bone Regeneration, Mineralization, Surface Modification, Functional Coatings

ÖZET

KEMİK DOKU REJENERASYONU İÇİN KENDİLİĞİNDEN TOPLANAN BİYOMİMETİK PEPTİT NANOFİBERLER

Samet Kocabey

Malzeme Bilimi ve Nanoteknoloji Programı, Yüksek Lisans

Tez Yöneticisi: Yar. Doç. Dr. Ayşe Begüm Tekinay

Ağustos 2012

Kendiliğinden toplanan peptit nanofiberler; çok yönlü, biyofonksiyonel ve hücrelerarası iskeleyi taklit edebilen yapılarından dolayı rejeneratif tıp alanında sıklıkla kullanılmaktadır. Bu yapılar sayesinde kemik doku rejenerasyonu uygulamalarında kullanılmak üzere osteokondüktif ve osteoindüktif peptit nanofiberler elde edilebilmektedir. Bu tezde, hücrelerarası iskeleyi taklit eden peptit nanofiberlerden oluşan iki boyutlu jellerin kullanılması ve titanyum implentlerin fonksiyonelleştirilmesi gibi iki farklı yaklaşım kullanılarak kemik doku rejenerasyonu ve mineralizasyonu amaçlanmıştır. İlk olarak, hücrelerarası iskeleyi taklit eden peptit nanofiberlerin geliştirilmesi amaçlanmıştır. Bu sebeple, kemik hücrelerarası iskelesi yapısında bulunan glikozaminoglikanların kimyasal yapıları kullanılarak glikozaminoglikanları taklit edebilen peptit nanofiberler tasarlanmıştır. Glikozaminoglikan mimetik peptit nanofiberler,

osteojenik aktivitede çok önemli rolü olan BMP-2 büyüme faktörüyle etkileşim göstermiştir. Bu peptit nanofiberlerin glikozaminoglikanları taklit eden yapısı ve BMP-2 ile olan etkileşiminin, osteoblast hücrelerinin osteojenik aktivitesini ve mineralizasyonunu arttırdığı gözlemlenmiştir. ALP aktivitesi, Alizarin Red boyaması ve EDAX spektroskopisi sonuçları, peptit nanofiberlerin osteojenik hücrelerin mineralizasyonunu önemli ölçüde tetiklediğini göstermiştir.

Ayrıca, titanyum biyomedikal implentlerde meydana gelen kemik doku entegrasyon problemlerini önlemek için, midyelerin yapışma mekanizmasından faydalanarak, hibrit osteokondüktif peptit nanofiber sistemi geliştirilmiştir. Bu sebeple, Dopa molekülü konjuge edilmiş peptit amfifiller, osteojenik aktivite sağlayan biyolojik peptit sekansı içeren peptit amfifillerle beraber kullanılarak titanyum yüzeyleri biyofonksiyonel hale getirilmiştir. Dopa yoluyla yüzeye immobilize olan osteojenik peptit nanofiberler, implent ile osteoblast hücreleri arasında osteokondüktif bir ara yüzey oluşturmuştur ve bu yüzeyler kaplanmamış yüzeye kıyasla yumuşak doku oluşumuna sebebiyet veren fibroblastların bağlanma ve yaşamalarını inhibe etmiştir. Özet olarak, osteojenik hücrelerin osteojenik aktivite ve mineralizasyonunu tetikleyen osteoindüktif ve osteokondüktif peptit nanofiberler geliştirilmiştir. Geliştirilen biyoaktif peptit nanofiberler kemik doku mühendisliğinin klinik uygulamalarında kullanılmasında ümit vadetmektedir.

Anahtar Kelimeler: Peptit Nanofiberler, Biyomimetik, Kendiliğinden-Toplanma, Hücrelerarası İskele, Glikozaminoglikan, Kemik Rejenerasyonu, Mineralizasyon, Yüzey Modifikasyonu, Fonksiyonel Kaplama.

Acknowledgement

First of all, I very much appreciate spending two years in a great environment with nice people. I would like to thank my advisor, Prof. Ayşe Begüm Tekinay, for her help and advice at all times. She always pushed me to do my best and take my job seriously. Her advice not only scientific subjects but also in social issues prepared me for my future life. She disciplined me a lot. I would tender my thanks to my co-advisor, Prof. Mustafa Özgür Güler, for his help and guidance. I was inspired by him and he helped me to improve my view of science. I was lucky to work with my both advisors.

This work could not be accomplished without my friend and colleague, Hakan Ceylan. We did almost all the work together, by working day and night. We shared a lot. I would like to thank him for his help and companionship during two years.

I would like thank Hilal Unal for her support and for cheering me up all the time. I also would like to thank Seher Ustun for her friendship and help. I would like to thank Busra Mammadov for her help in many experiments.

It was great to know you and work with you: Aysegul Tombuloglu, Rashad Mammadov, Handan Acar, Turan Selman Erkal, Oya Ustahüseyin, Zeliha Soran, Ruslan Garifullin, Yavuz Selim Dağdaş, Selim Sülek, Gözde Uzunallı, Elif Duman, Arif Khaliliy, and Göksu Çınar. I would like to thank for their friendship and support.

I would like to thank UNAM (National Nanotechnology Research Center) to give me this opportunity and to thank TUBITAK (The Scientific and

Technological Research Council of Turkey) for financial support, BIDEB 2210 MSc fellowship, and grants 110M353 and 112T042.

I would like to thank my friend, Baran Canpolat, for his friendship, help and out-science activities.

I always feel the love and support of my family with me. I can’t thank them enough. I am so grateful to have such a great family.

Finally, I am very grateful to meet a special person, Aslıhan Ekim, she has always been with me and supported me all the time.

Table of Contents

List of Figures

Chapter 1
Introduction

1.1 Bone Structure and Properties

Bone has a highly hierarchical arrangement of both organic and inorganic materials in different levels of hierarchical structural organization. These levels are distinguished into five categories according to their sizes: macro structure, micro structure, sub-micro structure, nano-structure and sub-nano structure. [1-2] (Figure 1.1) The macro structure is formed by cancellous (trabecular) and cortical (compact) bone. While cortical part forms the dense outer layer of the bone, cancellous part forms the thin, reinforcing structure which is located inside the bone. Both types of bone can be distinguished by their degree of porosity and density. [3] The micro structure of the bone (10 – 500 μm) includes Haversian systems, osteons and single trabeculae. [4] Osteons or Haversian systems are formed by sheets of mineralized collagen fibers (lamella) wrapped in concentric lamella layers around a central canal. These structures look like a cylinder that is about 200-250 μm in diameter, aligning parallel to the long axis of the bone. [5] Sub-microstructure of the bone consists of lamellae whose thickness is generally between 3-7 μm. [6] Arrangements of lamellae can be changed due to the orientation of collagen fibrils inside, which is either longitudinal (along the long axis of lamellar sheet) or transverse (perpendicular to the long axis). [7] When bone structure is examined at nano-level (100 nm - 1 μm), it is seen that the structure is made up of collagen fibrils and embedded crystals. [8] The most

prominent structure at this level consists of collagen fibers surrounded and infiltrated by minerals which allows supra-molecules to attach on it. [9] At last, the sub-nano structures of bone consists of three main materials; collagens, crystals and non-collagenous organic proteins. The mature crystals are plate-shaped and generally located within collagen fibrils in discrete space which prevent growth by forcing them to be discrete and discontinuous. [4] They grow in a specific crystalline orientation parallel to the long axis of collagen fibrils. [10] The main component of the matrix is Type I collagen which is secreted by osteoblasts and self-assemble into fibrils with a specific tertiary structure. Non-collagenous organic proteins are phospho-proteins like osteocalcin, osteopontin, bone sialoprotein and osteonectin which function to regulate the orientation, size and crystal habits of the mineral deposits. [11] Moreover, they can serve as a reservoir for calcium and phosphate ions for mineral formation via chelation of calcium or enzymatic release of phosphorus from proteins.

1.2 Bone Tissue Engineering

Bone is a dynamic tissue that plays an integral role in locomotion, mechanical support, mineral ions homeostasis and protection of integral organs. [12] It consists of collagenous fibrous matrix wherein calcified hydroxyapatite crystals are oriented and aligned in a structurally organized manner. [13] Mineralization of the bone in this way provides a drastic strength whose elastic modulus varies between 14 – 20 Gpa. [8] Despite the high mechanical properties of bone, severe damages could occur due to external impacts, internal disfunctions or infections.

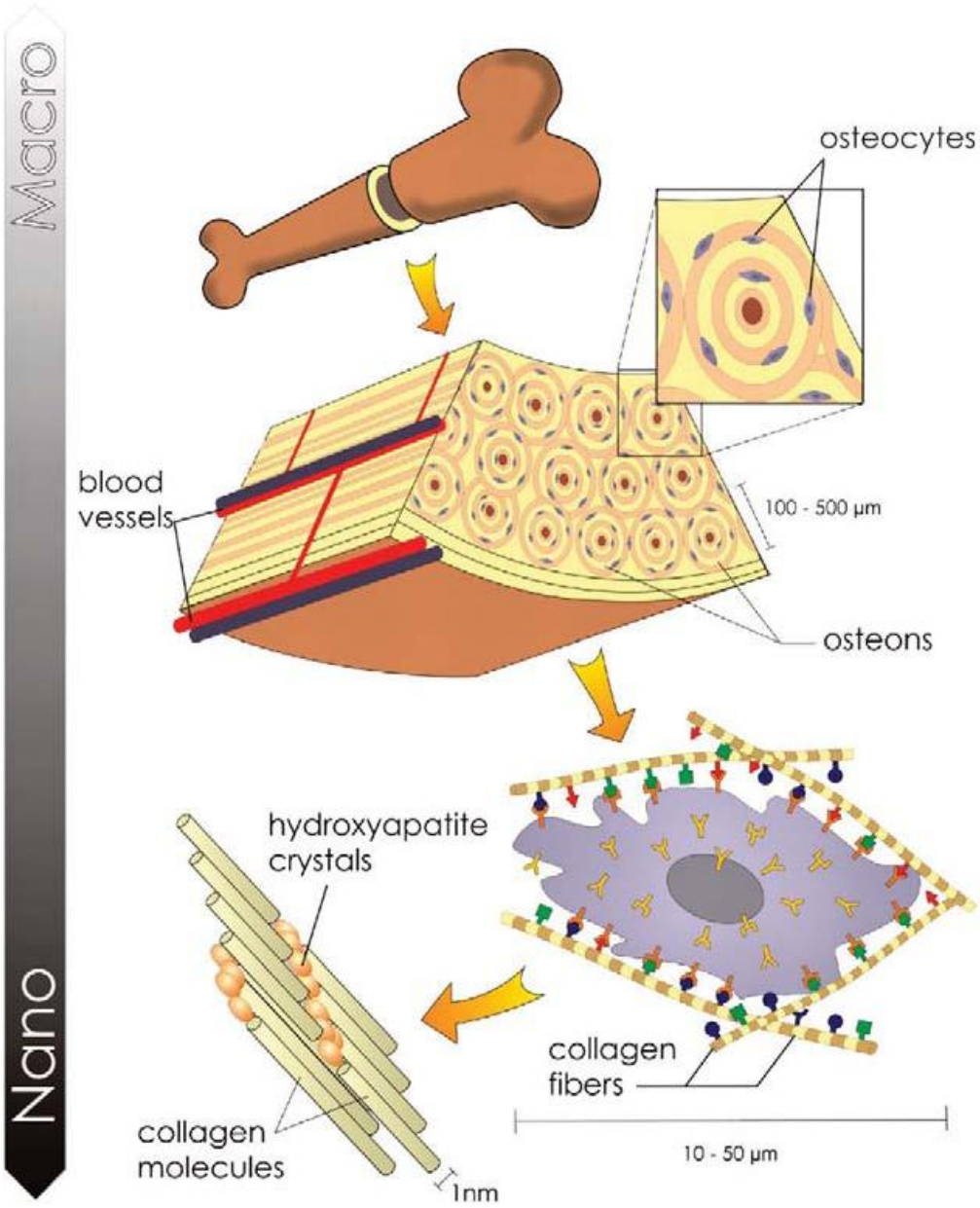

Figure 1.1 Hierarchical organization of bone from micro to nano length scales. a) Calcified compact outer layer which consists of b) many cylindirical Haversian systems, or osteons. c) Osteogenic cells interacting with extracellular matrix components through their cell surface receptors. d) Well-defined nano architecture of bone extracellular matrix. (Adapted with permission from Stevens et al. Materials Today, 2008, 11, 5)

Regenerative capacity of bone is relatively higher particularly in younger people which enables healing of tissue without any intervention. However, bone defects formed after tumor resections and non-union fractures require a template for oriented regeneration of bone tissue. These kinds of problems have been tried to be solved by using allografts, autografts or synthethic implants like ceramics or metals. [14] However such methods are far from ideal due to several difficulties associated with their applications. For instance, allografts taken from another donor can cause infection risk or immune rejection. Moreover, autografts can cause severe pain or morbidity at the part of donation and synthetic materials can generate biocompatibilty and biodegredability problems that can end up with inflammation and auto-immune disorders. [15-18] To overcome these limitations, researchers have developed novel tissue engineering systems for bone regeneration by mimicking natural environments of cells including extracellular matrix and its collageneous components while providing sufficient mechanical support for regenerating tissue. Thus, they opened the door to construct porous scaffolds where cells adhere, migrate, proliferate and differentiate by using signaling mechanisms. At the beginning, first generation materials were used in bone tissue engineering applications. For this purpose, different hydrogels were developed from both natural polymers such as collagen, chitosan, gelatin and synthetic polymers like poly-methacrylate and PEG. [19] These synthetic materials are biocompatible but they lack bioactivity. Then, second generation materials were developed to meet bioactivity where tissue implantation elicited regeneration response. For this purpose, biomimetic materials were developed to

mimic several aspects of the existent tissue. [20] Hydroxyapatite can be given as an example to second generation materials which is found in bone and teeth. Although these materials provide biocompatible and bioactive features, signals to control cellular behaviors at molecular level is required to create an environment for complete bone tissue regeneration as in natural bone. To achieve this task, third generation materials, hydrogels with further modifications such as biofunctional groups or growth factors were created to improve bone regeneration. [21] Self-assembled peptide amphiphiles, an example of these materials provide extracellular matrix mimicking properties and biofunctionality in addition to their versatile structures. [22] Previous studies have proved enhanced contribution of these assembled nano structures to biomineralization through nucleation of hydroxyapatite crystals on the surface of nanofibers. [23] While designing these engineered constructs, mechanical characteristics of the hydrogels such as strength, porosity, pH and thermo-tunability should be taken into consideration since they have a direct effect on osteogenesis and biomineralization. [24]

The following section is an overview of the different approaches used in bone tissue engineering. In the first part, material-based approaches were covered. Biomaterials used in bone regeneration were discussed as various hydrogels including biological, synthetic, injectable polymers and self-assembled peptide amphiphiles with biofunctional groups. In the second part, cell based strategies were mentioned including stem cells and progenitor cells. In the final part, growth factor based approaches were discussed.

1.3 Different Approaches used in Bone Tissue Engineering

1.3.1. Material-Based Approaches

Biological polymers are highly preferred in bone regeneration and replacement procedures due to innate biological information they provide to the cells. Thus, cellular attachment and chemotaxis can be induced by these biological signals. These materials are derived from natural polymers such as collagen, hyaluronic acid, gelatin (degraded form of collagen), fibrin, chitin and its deacetylated derivative chitosan. [25] They are advantageous because of their biodegradability and high biocompatibility. However, there are still existing concerns about potential risk of disease transmission, immunogenecity and weak mechanical properties. In order to recapitulate organic and inorganic phase of bone structure, these materials are generally utilized in combination with bioactive inorganic materials consisting of calcium phosphate and hydroxyapatite. [26] Previous studies have shown that composites of natural polymers are capable of inducing osteogenesis. [27] Among these materials, collagen constitutes the main phase of bone. Since it is degraded enzymatically, different forms like sponges and fibers can be easily processed. [28] In a study conducted by Zou and his group, collagen hydrogel combined with an inorganic calcium phosphate was used as a scaffold and collagen fibrils were cross-linked using gluteraldehyde. It was reported that these hybrid scaffolds enhanced bone tissue regeneration after 12 weeks of implantation into animals. [29] Fibrin glue, another naturally derived analogue of the blood coagulation process, is commonly used as a tissue adhesive reagent due

to its favorable biological behavior. [30] Le Nihouannen et al. benefited from fibrin's biocompatible and bioadhesive features and combined this material with macroporous biphasic calcium phosphate granules to increase biomineralization in fibrous network. [31] Gelatin, degraded version of the collagen, is another material used in biomineralization and calcification experiments. Its insufficient bioactivity could be enhanced by mixing with inorganic materials. To achieve this task, Sander et al. designed gelatin microspheres incorporated with calcium phosphate nanocrystals. It was observed that calcifying capacity of these composite particles are much better than the inert gelatin materials. [32] Chitosan, a polysaccaride formed by deacetylation of chitin, which is the main structural component of the crustacean exoskeletons, is highly preferred in bone experiments as it has noteworthy wound healing properties, low immunogenicity and intrinsic anti-bacterial activity. [33] Combination of this material with inorganic materials like calcium phospate [34] and hydroxiapatite [35] results in bioactive composites which demonstrates osteoconductivity and enhanced biomineralization. [36] Extracellular matrix mimicking and cell function directing properties of this material make it more favorable in bone tissue engineering applications. For this reason, Wang et al. combined chitosan and collagen composites with β-glycerophospate to induce mineralization. They found out that presence of chitosan in these materials resulted in higher expression of bone specific osterix and sialoprotein genes. [24]

In order to extend current concept of scaffolds and obtain three-dimensional scaffolds, synthetic polymers are utilized in bone regeneration applications.

These polymers have versatile characteristics [37] and can be processed using several techniques such as gas foaming, phase separation and porogen leaching. [38-39] Moreover, it is possible to adjust their structures using different monomer units. Although naturally derived polymers are desirably functional, they lack reproducibility due to their natural origin such as molecular weight of these materials are widely distributed and they have short half lives [40] For these reasons, synthetic polymers can be advantageous over naturally derived ones when combined and tailored alone or with other monomers. Such a combination contributes to tunable characteristics including swelling ratio, mechanical strength, and porosity and surface properties. [41] Cross-linking techniques are highly favorable in polymerization processes like photo-polymerization or radical-polymerization and thus forming hydrogels for biomineralization. Commonly used synthetic hydrogels for bone regeneration are PEG (poly ethylene glycol), poly (2-hydroxyethyl methacrylate) (pHEMA), PLA, PGA, PLGA(copolymers of PGA and PLGA) and NIPA. [42-43] Sarvestani et al. used PEG-based hydrogels as a matrix and combined them with inorganic hydroxyapatite nanoparticles by using glutamic acid rich linker to enhance interaction between them. [44] Another way to develop pHEMA composite materials is to use hydroxyapatite crystals. Their ability to promote osteoblastic differentiation thus biomineralization has been proved. For this purpose, Song et al. applied this material in bone defects and benefited from elastomeric properties of the material in implanting process. [45] On the other hand, NIPA can also be utilized as hydrogels after copolymerizing with other chemicals. Although this

polymer is liquid at room temperature, when the temperature is increased to 37 °C, it makes transition from solution to gel form. Mujumdar SK et al. copolymerized NIPA with dimethylaminoethylmethacrylate to produce mechanically strong composite hydrogels for bone tissue engineering applications. [46]

Over time, hydrogels made of injectable polymers became advantageous over other hydrogels that are only used via implantation or other surgical experiments. With the help of tunable chemical properties of polymers, injectable hydrogels are regarded as promising tools in bone tissue engineering applications. Simple and effective extracellular matrix mimicking scaffolds can be designed with injectable properties. These scaffolds are either modified from naturally derived materials like gelatin, hyaluronan and chondroitin sulfate or formed by adding functional cross-linkers to the synthetic polymers like NIPA. [47-48] In both ways chemical modification takes place such as thiolation of biomacromonomers with poly ethylene glycol diacrylate or reversible addition of polyacrylate groups to the polymers. Different composition experiments were also performed to make injectable hydrogels. Tan et al. designed an injectable hydrogel consisting of calcium alginate and nano-HA. [49] The injectability of material was adjusted by altering the relative concentrations of components. β-hairpin peptide based hydrogels have also potential use in injectable therapies. These solid gels can shear-thin and consequently flow under a proper shear stress. However, they immediately recover back into a solid when stress is removed. This property of hydrogel makes it favorable in bone tissue engineering applications. [50]

Self-assembled peptide amphiphiles were designed to overcome bioactivity and biofunctionality problems, at which other synthetic or naturally derived hydrogels fall short. They are capable of self-assembling into well defined nanofibers which display specific bioactive epitopes to control cell behavior for biomineralization and bone regeneration. [23] It is shown in the previous experiments that peptide amphiphile nanofibers with phosphoserine residues promoted nucleation of hydroxyapatite crystals on the long c – axis of collagen fibrils parallel to nanofibers. [51] By using co-assembly of two PA molecules, combined effect on both bioactivity of the fibronectin epitope RGDS and the phosphoserine residues for hydroxyapatite nucleation were obtained in orthotopic rat femoral critical-size defect models. [52] (Figure 1.2) Moreover, these three-dimensional biomimetic systems, which resemble extracellular matrix, promoted bone regeneration in vivo. Peptide amphiphiles can be further modified with bioactive sequences which are inspired from epitopes of extracellular matrix proteins that allows cell adhesion, induction and differentiation. RGDS ligand is commonly used for this purpose which is prevalent in many extracellular matrix proteins including fibronectin, laminin and osteopontin, and it has been well documented for directing general cell adhesion. [53] The KRSR peptide sequence, binds to transmembrane proteoglycans and has been found to selectively increase osteoblast adhesion when functionalized with other bioadhesive moieties. [54] Another one, DGEA is a collagen type I adhesive peptide sequence and exhibits specific binding for osteoblasts via the alpha2-beta1 integrin. Thus, it increases osteogenic differentiation of mesenchymal stem cells. [55] To increase

biodegradability in scaffolds which are made up of peptide amphiphiles, GTAGLIGQ amino acid sequence that is sensitive to MMP-2 was utilized. This motif provides cell-mediated proteolytic degradation of the nanofiber network which allows cell migration through the matrix and eventual remodeling of the natural extracellular matrix. [56]

1.3.2 Cell-Based Approaches

Cell based approaches mainly involve implantation of osteogenic cells or cells with osteogenic differentiation capacity like primary osteoblasts, osteoprogenitor cells and stem cells. Currently used osteoblasts and osteoprogenitor cells are isolated from bone, expanded in culture and differentiated before usage. On the other hand, stem cells are isolated from fresh bone marrow or other cell sources such as adipose tissue. Previous studies have proven the positive effect of implanting osteogenic cells into defect sites on bone regeneration. [57] To illustrate, Werntz et al. has indicated that combining these cells with a collagen scaffold in a rat model showed similar mechanical and functional properties to autologous bone grafts thus accelerated the healing process of a segmental bone defect. [58] The other widely utilized cell type, mesenchymal stem cells are categorized as multipotent stem cells due to their high potential to differentiate into multiple lineages. Their potential to give rise to osteogenic cells and regenerate injured tissue make them key players in bone regeneration process. [59] Previous in vivo studies have demonstrated that integrating biomaterials with these highly plastic cells and subsequent implantation of these constructs give promising results in formation of bone and increase in osseointegration.

Yoshikawa et al. cultured rat bone marrow stromal cells on hydroxyapatite cubes in the presence of ostegenic media and subsequently implanted these constructs into syngeneic rats. [60] After fifty-two weeks, a constant osteogenesis with active bone remodeling process was observed. As an alternative to cell-based approaches researchers started to use genetically modified cells which have osteoinductive capacity due to the addition of osteogenic genes. Fibroblasts are one of the common used cells for genetic modification, because they can be easily harvested, expanded in culture and transfected with desired genes. Previous studies have pointed out that using genetically modified dermal fibroblasts that overexpress osteoinductive genes including Runx2/Cbfa1 and LMP-1 induced osteoblastic differentiation, mineralization, and bone formation. [61-62] Moreover, mesenchymal stem cells were also transfected with osteogenic genes to induce bone regeneration. In the study conducted by Tsuda et al. BMP-2 gene was efficiently transferred to mesenchymal stem cells and induced osteogenic differentiation in vitro. [63]

1.3.3 Growth factor-Based Approaches

In bone regeneration and osteogenic differentiation, bone morphogenic proteins (BMPs) are of particular interest related to crucial role in embryological bone formation, osteoinduction and bone repair. [64-67] Although many proteins belong to this family, BMP-2 and BMP-7 are highlighted in inducing bone formation by mimicking endochondral ossification at ectopic sites in a rat model by Wang and Sampath. [68-69] Delivery systems for these growth factors are highly favorable by using demineralized bone matrix, collagen composites,

calcium phosphates, hydroxyapatite and PLGA like polymers in order to repair bone defects. [70] To increase release efficiency, release time and to prevent these growth factors from being degraded end-functionalized heparin like molecules had potential use in recent studies. For this purpose, biotin-end functionalized ROMP polymers were used as proteoglycan mimetics of chondroitin sulfate polymers to capture and release growth factors in Song Gil Lee's research. [71] (Figure 1.3) In another research, this application was developed further by using star-PEGs to encapsulate growth factors in a highly organized manner to increase release time using scaffolds. In addition to growth factors, specific peptide sequences which mimicked BMP binding regions of proteoglycans have been used in osteogenic differentiation and osteoinduction. [72]

1.4 Motivation and Goals

To achieve bone regeneration in an orchestrated fashion, all of the approaches mentioned previously should be combined in a smart scaffold system, which has osteoconductive and osteoinductive features that is supported with an appropriate cell source and growth factors. At this point, self-assembled peptide nanofibers are regarded as promising tools due to their strong osteoconductive and osteinductive properties. In this thesis, cellular response on peptide nanofiber systems was explored to develop multifunctional tissue engineering constructs. In the first chapter, I discussed biomimetic peptide amphiphiles which were designed to mimic glycosaminoglycans and used together with osteoinductive

growth factors for mineralization. In the second chapter, I focused on adhesive and osteogenic peptide amphiphiles and their effect on osteogenic activity of cells after coating on titanium implants.

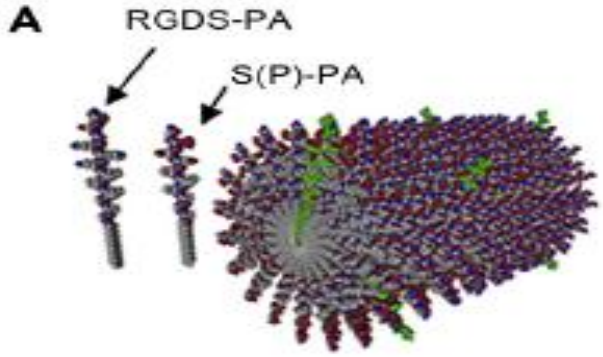

Figure 1.2 Molecular graphics representation of self-assembled nanofiber formed by co-assembly of phosphorylated serine PA and the RGDS-PA. (Adapted with permission from Mata.A. et al. Biomaterials, 2010, 31(23), 6004-12)

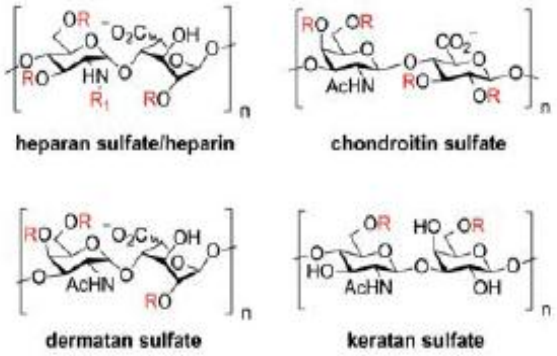

Figure 1.3 Structures of GAG classes used in BMP like growth factors encapsulation and release. (Adapted with permission from S.G. Lee et al. Chemical Science, 2010, 1(3), 322-325)

Chapter 2

Glycosaminoglycan Mimetic Peptide Nanofibers for Biomineralization

Part of this study was submitted to be published as "Glycosaminoglycan-Mimetic Peptide Nanofibers Promote Mineralization by Osteogenic Cells" Samet Kocabey, Hakan Ceylan, Ayse B. Tekinay and Mustafa O. Guler.

2.1 Introduction

Bone regeneration at the side of injury requires proper communication of cells with surrounding area. To meet these requirements, an osteoconductive biomaterial scaffold, a cell source with osteogenic properties and osteoinductive growth factors are used in a synergistic manner. Extracellular matrix consists of numerous type of molecules such as collagenous and noncollagenous proteins to regulate cellular behavior by promoting cell adhesion, proliferation, migration and differentiation through activating specific sets of genes that regulate various signaling pathways. [73-75] Extracellular matrix in bone tissue is composed of approximately 50-70% of inorganic calcium and phosphate minerals, and 20-40% of organic components, which mainly consist of collagen type I surrounded by proteoglycans, glycosaminoglycans and other proteins. [76] Glycosaminoglycans that constitute major organic component of ECM have significant roles during bone regeneration. They can affect cellular behaviors either by directly interacting with cell surface molecules or by encapsulating and

stabilizing growth factors and enhancing their interactions with targeting receptors. [77] Recently, glycosaminoglycans were shown to enhance osteoblast differentiation of bone marrow derived human mesenchymal stem cells. [78] The composition and spatial organization of glycosaminoglycans can vary for each tissue type depending on the chemical groups on their chains like sulfate and carboxylate. Bone extracellular matrix contains a variety of sulfated and unsulfated glycosaminoglycans including chondroitin sulfate, dermatan sulfate and hyaluronan; while heparin and heparan sulfate are mostly found in bone marrow. [79-81] These glycosaminoglycans can trigger bone remodeling through affecting cellular proliferation and differentiation via growth factor mediated signaling or direct cell surface interactions. In previous studies, chondroitin sulfate containing artificial biomimetic scaffold was demonstrated to induce osteoblast differentiation of MSCs specifically. [82] Moreover, over-sulfated chondroitin was shown to promote collagen deposition, alkaline phosphatase activity and mineral accumulation of osteoblasts. [83] Synthetic materials made of sulfated hyaluronan also increased TNAP activity and formation of osteoblastic cell aggregates. [84]

In addition to the interaction between glycosaminoglycans and cells, growth factors cooperating with glycosaminoglycans are also crucial determinants of bone regeneration. Glycosaminoglycans have been previously shown to interact with a large number of bone-regulating proteins and cytokines such as TNF-alpha, BMPs, OPG, RANKL and other members of TGF-β. [85-88] Among them, BMP-2 is one of the most osteoinductive growth factors which induces

osteogenic differentiation of multipotent mesenchymal stem cells and directs bone formation in both animals and humans. [89-92] Binding of BMP-2 to glycosaminoglycans found in the extracellular matrix synergistically enhances the osteogenic activity of cells. When used with high sulfated heparin, the specific activity of this protein increases about five-fold. [93] Besides, increasing biological activity of BMP-2, glycosaminoglycans also serve as potential carriers by capturing and increasing the local concentration of proteins. [94] In a previous work, binding of BMP-2 to immobilized heparin was shown the increase osteogenic activity of MG-63 osteoblasts. [95]

Since ECM plays an important role on bone regeneration, using ECM resembling structures are highly preferred by researchers. [96] In previous studies, natural ECM extracted from animal tissues was used as a scaffold for bone replacement. [97-98] However, this type of approach could cause immunological response or disease transmission. Self-assembled peptide amphiphiles are versatile structures which can be decorated to mimic extracellular matrix components. Their ability to form collagen like fiber structures and representation of biological cues on these structures make them promising tools for bone tissue engineering applications. In a previous work, Stupp and co-workers designed osteoconductive phosphoserine bearing peptide amphiphiles for mineralization with similar alignment observed between collagen and hydroxyapatite crystals in bone. [23] A variety of ECM-derived peptides such as DGEA and KRSR or growth factor derived peptides like BMP-

2 were also represented on peptide amphiphiles to be used in bone regeneration and mineralization studies. [52, 54, 72]

This chapter presents utilization of glycosaminoglycan-mimetic self-assembled peptide nanofibers for the purpose of mineralization of osteogenic cells. These peptide amphiphiles resemble the structure of glycosaminoglycans found in natural extracellular matrix. I describe below the design and characterization of glycosaminoglycan-mimetic peptide nanofibers, their BMP-2 binding abilities and the affect of these nanofibers on osteogenic cell behaviors such as viability, proliferation and mineralization.

2.2 Experimental

2.2.1 Synthesis of Glycosaminoglycan-mimetic Peptide Amphiphiles

To synthesize glycosaminoglycan-mimetic peptide amphiphiles, solid phase peptide synthesis was performed with standard Fmoc chemistry. Rink Amide MBHA resin or Fmoc-Glu(OtBu)-Wang resin was used as template where amino acids were added on. Amino acid couplings were performed as 2 equivalents of amino acids activated with 1.95 equivalents of HBTU and 3 equivalents of DIEA for 2 h. To remove Fmoc protection groups, 20% piperidine–dimethylformamide (DMF) solution was used for 20 min. To permanently acetylate the unreacted amine groups after each coupling step 10% acetic anhydride–DMF solution was used. DMF and dichloromethane (DCM) were used as washing solvents after each step. To synthesize sulfonated PAs, p-sulfobenzoic acid was added to the side chain of lysine which has -4-methytrityl

(Mtt) side chain protection as used for selective deprotection of amine groups. Mtt removal was performed by shaking resin for 5 min with TFA:TIS:H_2O:DCM in the ratio of 5:2.5:2.5:90. Cleavage of the PAs and protection groups from the resin was performed by using a mixture of TFA:TIS:H_2O in the ratio of 95:2.5:2.5 for 3 h. Rotary evaporation was used to remove excess TFA from the peptide solution. PAs in the remaining solution were precipitated in ice-cold diethyl ether overnight. Next day, the precipitate was collected by centrifugation and dissolved in ultrapure water. This solution was frozen at -80 °C for 4 h and then lyophilized for 4-5 days.

2.2.2 Mass Spectrometry and HPLC Purification

To characterize synthesized peptide amphiphiles, a quadruple time of flight (Q-TOF) mass spectrometer with electrospray ionization (ESI) source equipped with a reverse-phase analytical high performance liquid chromatography (HPLC) was used. Agilent Zorbax Extend-C18 2.1 x 50 mm column was used for negatively charged peptide molecules and Zorbax SB-C8 4.6 x 100 mm column was used for positively charged peptide molecules respectively. A gradient of water (0.1% formic acid and 0.1% NH_4OH) and acetonitrile (0.1% formic acid and 0.1% NH_4OH) were used for liquid chromatography. In order to purify synthesized peptide amphiphiles, reverse-phase preparative HPLC equipped with Zorbax Extend-C18 21.2 x 150 mm column for negatively charged peptide molecules and Zorbax SB-C8 21.2 x 150 mm column for positively charged peptide molecules was used. A gradient of water (0.1% TFA and 0.1% NH_4OH) and acetonitrile (0.1% TFA and 0.1% NH_4OH) were used.

Furthermore, positively-charged peptide amphiphiles were treated with 0.1 M HCl solution in order to remove residual TFA at the end.

2.2.3 Characterizations of Self-Assembled Peptide Nanostructures

Chemical and mechanical characterizations of peptide amphiphiles were performed using SEM, TEM, CD, FT-IR and rheology. To visualize nanofiber formation upon self assembly of peptide amphiphiles, SEM and TEM imaging were performed. For SEM imaging, 30-40 μL of 1% PA mixtures (SO_3-PA/K-PA and E-PA/K-PA) were placed onto silicon wafers and critical point dried after dehydrating sequentially in 20%, 40%, 60%, 80% and 100% ethanol. Samples were coated with 5 nm Au-Pd and imaging was performed using SEM (FEI Quanta 200 FEG) with ETD detector at high vacuum mode at 10 keV beam energy. For TEM imaging, a Lacey mesh ultrathin carbon coated copper grid was used. The upper part of grid was dipped into 1% PA mixtures (SO_3-PA/K-PA and E-PA/K-PA) for 1 min and dried in fume hood for at least 30 min. Imaging was performed using FEI Tecnai G2 F30 transmission electron microscope. In order to reveal secondary structure of peptide nanofibers, circular dichroism (CD) was performed using JASCO J815 CD spectropolarimeter. PA solutions were prepared in the range of 1×10^{-5} M – 3×10^{-5} M. All measurements were performed with three accumulations from 300 nm to 190 nm wavelength. Quartz cuvettes with 1 mm path length were used for measurements. For obtaining FT-IR spectra, 1% PA mixtures were prepared, lyophilized and powdered. Then, 1 mg of PA mixture was completely mixed with 99 mg KBr. The mixture was then pressed between two stainless steel disks

by applying hydraulic press up to 7 atm. The FT-IR measurement was performed using Bruker Tenson 27 FT-IR spectrometer at the transmittance mode. Mechanical properties of peptide nanofibers were quantified using Anton Paar Physica RM301 Rheometer operating with a 25 mm parallel plate configuration at 25 °C. 1 mM PA mixtures were prepared and adjusted as to completely fill 0.5 mm gap size. (245 µL volume of PA mixture is required to fill the gap completely) Frequency sweep measurement was performed by scanning storage modulus and loss modulus values from 100 rad/s to 0.1 rad/s of angular frequency with a 0.5% sheer stress.

2.2.4 Cell Culture

In order to perform 2D cell culture experiments, 1 mM PA solutions were prepared for glycosaminoglycan-mimetic peptide amphiphiles, SO_3-PA, E-PA and gelator K-PA. For coating, SO_3-PA and K-PA were mixed at 1:3 molar ratio, whereas E-PA and K-PA were mixed at 1:2 ratio to neutralize total charge during self-assembly. Same concentrations of SO_3-PA and E-PA were used for all experiments.

Saos-2 cells (human osteosarcoma cell line, ATCC^{R} HTB-85^{TM}) were used in all cell culture experiments. Cells were incubated at 37 °C in a humidified atmosphere supplied with 5% CO_2. Cell maintenance was provided in DMEM (Dulbecco's modified eagle's medium) supplemented with 10% FBS, 1% Penicillin/Streptomycin and 2 mM L-Glutamine. Cell culture was performed in 75 cm^2 flasks and cells were subcultured up to 1:8 ratio when 90% confluency was reached. Cell media was replenished every 3-4 days.

In mineralization experiments, the growth medium of cells was changed with osteogenic media after over-confluency which included DMEM 10% FBS supplemented with 10 mM β-glycerophosphate, 50 µg/mL ascorbic acid and 10 nM dexamethasone.

2.2.5 Cell Viability and Proliferation

To perform cell viability and proliferation analyses, cells were seeded on PA-coated and uncoated 24 well plates at a density of 5 x 10^3 cells/cm^2. At 1, 3 and 5 days after incubation, medium of cells was discarded, cells were washed with PBS once and then they were stained with 2 µM Calcein in PBS for 30 min at room temperature. Finally, at least 5 images/well were taken at 10x magnification by using fluorescent microscope for both qualitative and quantitative analysis. For quantification, they were counted by using Image-J software.

2.2.6 Cell Morphology

The morphology of cells was analyzed by using SEM (FEI Quanta 200 FEG) with ETD detector at high vacuum mode at 10 keV beam energy. Cells were seeded on 13 mm glass surfaces which were coated with 1 mM PAs (1:3 and 1:2 ratios respectively) and 5 x 10^3 cells/cm^2 density in growth medium. 3 days after incubation, cell medium was discarded and cells were washed with PBS once. Then, cells were fixed with 2% gluteraldehyde/PBS for 2 hrs in fume hood. After fixation, cells were washed with PBS once and then dehydrated sequentially in 20%, 40%, 60%, 80% and 100% ethanol. Before imaging, fixed

cells were critical point dried in Autosamdri® - 815B Tousimis and coated with 5 nm Au-Pd.

2.2.7 BMP-2 Binding Assay

To test the binding affinity of BMP-2 to peptide nanofibers, ELISA plates were coated with 1 mM and 0.1 mM PAs (1:3 ratio for SO_3-PA/K-PA and 1:2 ratio for E-PA/K-PA respectively). Equal volume (25 µL / well) of PAs were used for both SO_3-PA and E-PA, and volume of K-PA was adjusted according to them. After coating, samples were kept in 4 °C overnight. Next day, wells were washed with wash buffer (Tween-20/PBS) three times and blocked with 300 µL, 1% BSA blocking solution for 2 hrs. After blocking step, wells were washed with wash buffer and then 100 µL BMP-2 solution was added on wells at 100 ng/mL and 10 ng/mL concentrations (only PBS was used as background control) for 1 hr. Then, 100 µL biotinylated anti-BMP-2 antibody at 2 µg/mL concentration was added to the wells and incubated for 1.5 hr at 37 °C. Washing step with wash buffer was repeated. Then, 100 µL Streptavidin-HRP (1:200 dilution) solution was added and incubated for 20 min in the dark room. Washing step was performed again and 100 µL TMB substrate was added to each well. The plate was incubated at room temperature for 20 min in dark room. Finally, 50 µL stop solution was added to each well and optical density was measured after 30 min incubation at 450 nm by subtracting the reading at 540 nm.

2.2.8 Alkaline Phosphatase Activity Assay

In order to investigate ALP activity of Saos-2 cells, cells were seeded on PA coated and bare 48 well plates at a ratio of 3 x 10^4 cells / cm^2 in growth medium. Next day, medium was changed with osteogenic medium with or without BMP-2. At predetermined time points which were generally 1, 3, 7 and 10 days after osteogenic medium addition, medium was discarded and cells were washed with PBS once. Then, protein extraction was performed by adding M-PER Protein Extraction Kit (Thermo)/5% Protease Inhibitor solution as 150 µL/well for 30 min on shaker. Protein containing solutions were taken from each well by pipetting and transferred into eppendorf tubes. Then, protein samples in eppendorf tubes were centrifuged at 14000 g for 10 min, supernatants that contain proteins were taken and BCA protein assay was performed to quantify protein amount obtained from cells as described in manufacturer's protocol.

ALP activity was analyzed by measuring the colorimetric product of p-nitrophenol from endogenous ALP reaction. To do this, 50 µL of protein sample was taken from each sample and incubated with 150 µL of p-nitrophenol phosphate substrate in 96-well plates for 30 min on shaker. Serial dilutions of p-nitrophenol in 0.25 M NaOH were used as standards. Finally, optical density was determined at 405 nm wavelength by using a microplate reader. The ALP values were normalized to total protein amount regarding incubation time of samples with ALP substrate.

2.2.9 Alizarin Red-S Staining

To perform Alizarin Red-S staining, cells were seeded on PA coated and bare 48 well plates at a ratio of 3 x 10^4 cells / cm^2 in growth medium. Next day, cell medium was changed with osteogenic medium with or without BMP-2. Calcium deposition was assessed by staining with Alizarin Red-S after 14 days of incubation of cells in osteogenic medium. Briefly, cells were washed with PBS and fixed with ice-cold ethanol for 1 h at room temperature. Then, fixed cells were washed with distilled water first and stained with 40 mM Alizarin Red-S solution (pH 4.2) for 30 min at room temperature on shaker. After washing 4-5 times with distilled water to get rid of nonspecific binding, the stained calcium nodules were observed under a light microscope by using 10 x magnification.

2.2.10 EDAX Spectroscopy

All EDAX spectra were collected using ETD detector connected to a FEI Quanta 200 FEG scanning electron microscope. The electron beam was scanned over an area at 80x magnification for all samples to obtain chemical composition.

2.3 Results and Discussion

2.3.1 Design and Synthesis of Glycosaminoglycan-mimetic PA's

Three different peptide amphiphile molecules were designed and synthesized by solid phase peptide synthesis to form nanofibers and develop extracellular matrix mimicking environment where chemical groups in GAG structure is presented on peptide nanofibers. Peptide amphiphiles were designed as a

composition of hydrophobic alkyl group, β-sheet driving group and charged group. Lauric acid added at the end of peptide gives a hydrophobic character to peptide amphiphile which triggers hydrophobic collapse during self-assembly. [99] For β-sheet forming part, four non-polar aminoacids were used; Val-Val-Ala-Gly (VVAG). To mimic sulfonated glycosaminoglycans, SO_3-PA (Lauryl-VVAG-EGDK (pbs)S-Am) was designed. Charged aminoacids used in this peptide amphiphile structure were glutamic acid (E), aspartic acid (D) to bear carboxyl (COO-) group; lysine (K) to add sulfonate group to its side chain and serine (S) for providing hydroxyl (OH-) group as in natural sulfonated glycosaminoglycans. To mimic unsulfonated glycosaminoglycans, E-PA (Lauryl-VVAGE-OH) with only one glutamic acid after VVAG sequence was designed. These peptide amphiphiles are negatively charged at neutral pH and they form gels upon decreasing pH or by adding positively charged peptide amphiphiles or ions. To form nanofibers with these peptide amphiphiles, positively charged K-PA (Lauryl-VVAGK-Am) was synthesized adding lysine aminoacid to N-terminus of peptide amphiphile. (Figure 2.1)

2.3.2 Mass Spectrometry and HPLC Purification

QTOF-LCMS was used to verify synthesized peptide amphiphiles accordingly. Expected masses were obtained for all PA molecules which are 1225 for SO_3-PA, 653 for E-PA and 651 for K-PA as seen in Figure 2.2. To get rid of impurities preparative- HPLC was applied to all peptide samples and peptide amphiphiles with 90% purity were obtained at the end.

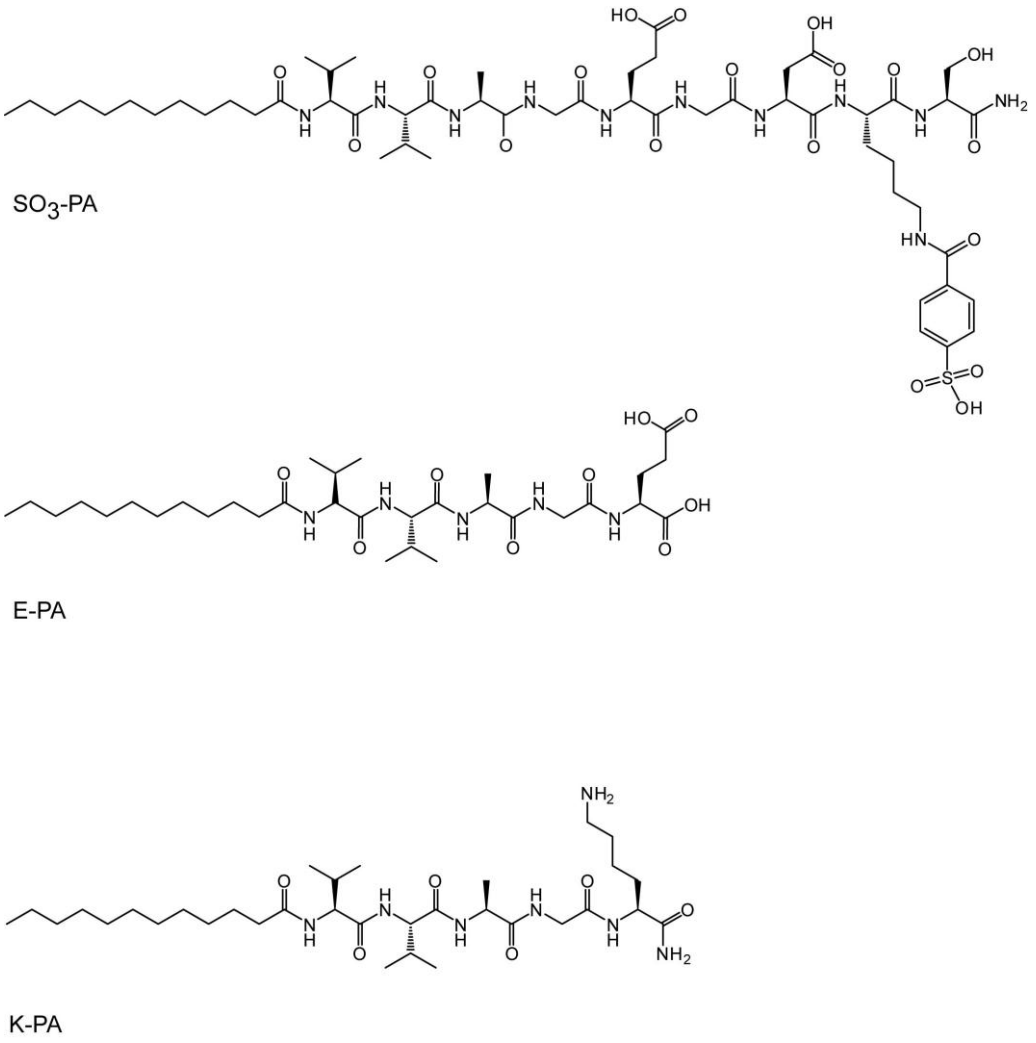

Figure 2.1 Chemical structures of synthesized peptide amphiphiles.

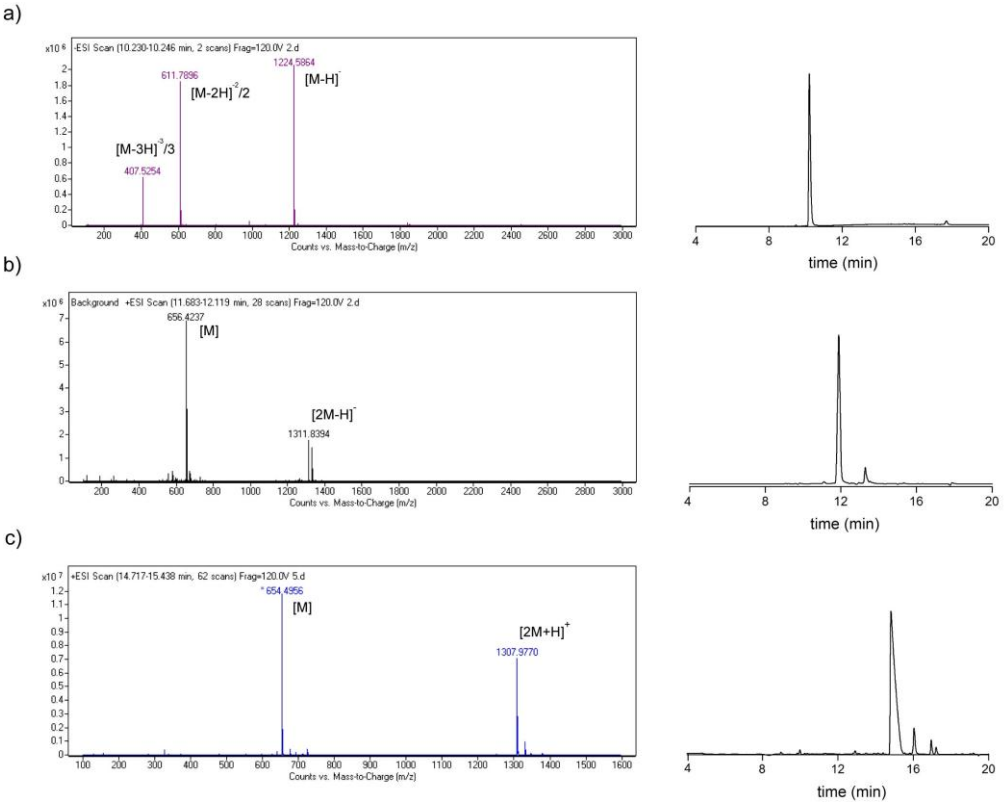

Figure 2.2 Mass spectra and liquid chromatograms of synthesized peptide amphiphiles. a) SO_3-PA, b) E-PA and c) K-PA.

2.3.3 Self-assembly and Characterization of Peptide Amphiphiles

2.3.3.1 SEM

To characterize self-assembly of peptide amphiphiles and nanofiber formation SEM imaging was performed. SEM imaging reveals that nanofibers formed upon mixing oppositely charged peptide amphiphiles, SO_3-PA/K-PA and E-PA/K-PA (Figure 2.3 a-b). These nanofibers resemble the native extracellular matrix structurally such that they are porous and they look like collagen fibers.

2.3.3.2 TEM

TEM imaging was also performed to further analyze nanofiber formation. TEM images revealed that nanofibers formed upon charge screening of oppositely charged peptide amphiphiles whose diameters change between 6 – 10 nm and lengths up to a few microns. (Figure 2.3 c-d) Moreover, bundling of nanofibers for both SO_3-PA/K-PA and E-PA/K-PA was also observed.

2.3.3.3 Circular Dichroism

To understand the secondary structure of peptide amphiphiles, Circular Dichroism (CD) was performed. CD measures the differential absorbance of left-handed and right-handed circularly polarized light which exhibited on optically active chiral molecules. In peptide amphiphile structure, the amide group forming the peptide backbone acts as a chromophore in the far UV region and provides the absorbance. SO_3-PA/K-PA and E-PA/K-PA nanofibers

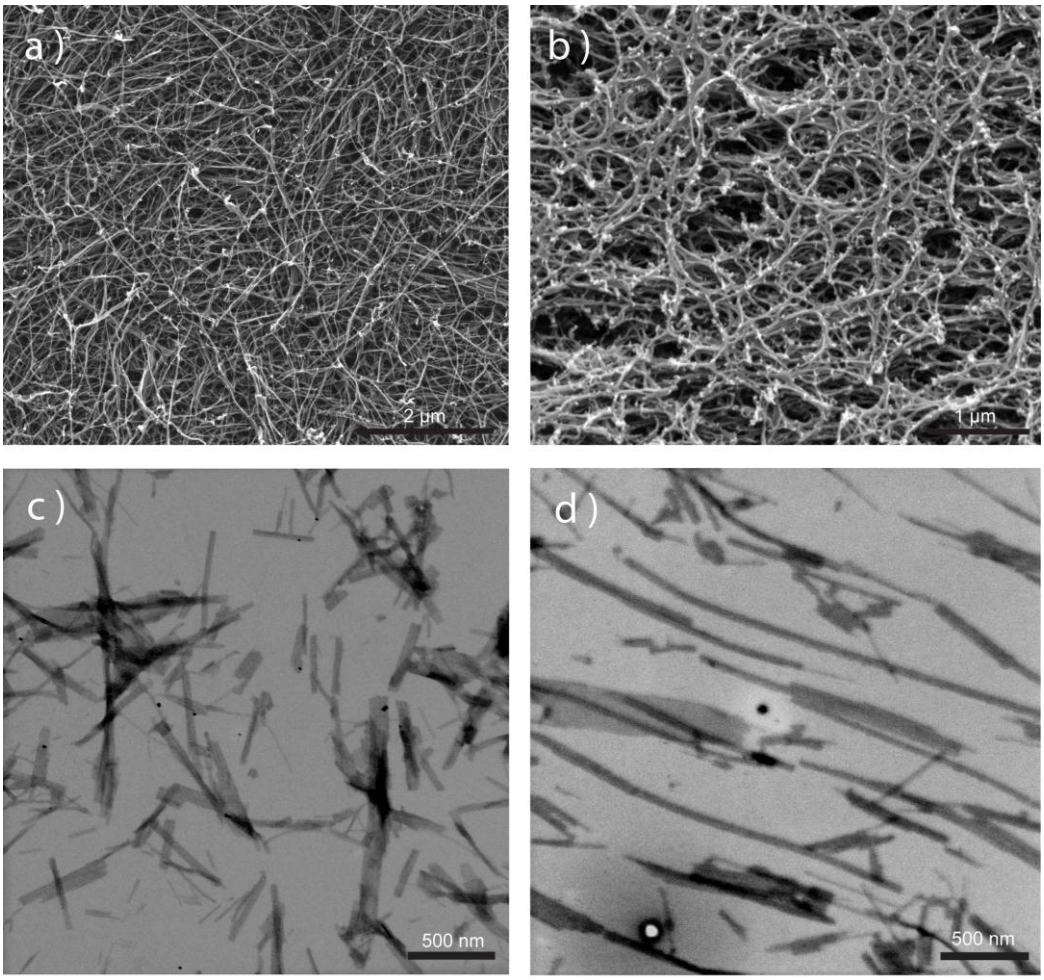

Figure 2.3 Microscopic characterizations of peptide amphiphiles. SEM images of peptide nanofibers formed at pH 7.4: a) SO_3-PA/K-PA and b) E-PA/K-PA. TEM images of peptide nanofibers formed at pH 7.4: c) SO_3-PA/K-PA and d) E-PA/K-PA.

clearly displayed positive maximum at around 200 nm and negative minimum at around 218 nm which proves the β-sheet driven self-assembly of peptide amphiphiles. However, no β-sheet structure was observed when peptide amphiphiles were used alone; they were just random noises instead. (Figure 2.4 a-b)

2.3.3.4 FT-IR

In order to characterize the formation of peptide nanofibers upon self-assembly, FT-IR spectra measurements were performed in the range of 1000 and 1800 cm^{-1}. In peptide structures, amide I is the most intense absorption band, which is characterized by the absorption governed by the stretching vibrations of the carbonyl (C=O) and amide (C-N) groups. The range is absorption is between 1600-1700 cm^{-1}, however the exact localization of the band centre is related to the secondary order of the structure. In our experiment, the amide I band was found to be centered to 1639 cm^{-1} for both SO_3-PA/K-PA and E-PA/K-PA nanofibers. (Figure 2.4 c) Absorption at this wavenumber indicates β-sheet-rich secondary structure. This observation is also consistent with the self-assembly-driven nanofiber formation by means of β-sheets between adjacent micelles and with the results of circular dichroism measurements. Amide II is characterized by absorption in the range of 1490 to 1600 cm^{-1}; which appeared at 1546 cm^{-1} in SO_3-PA/K-PA and E-PA/K-PA nanofibers. It mainly derives from N-H bending and C-N stretching vibrations. Absorption around 1043 cm^{-1} originating from S-O vibrations was a vibration signal of sulfonate group specific to SO_3-PA/K-PA nanofibers.

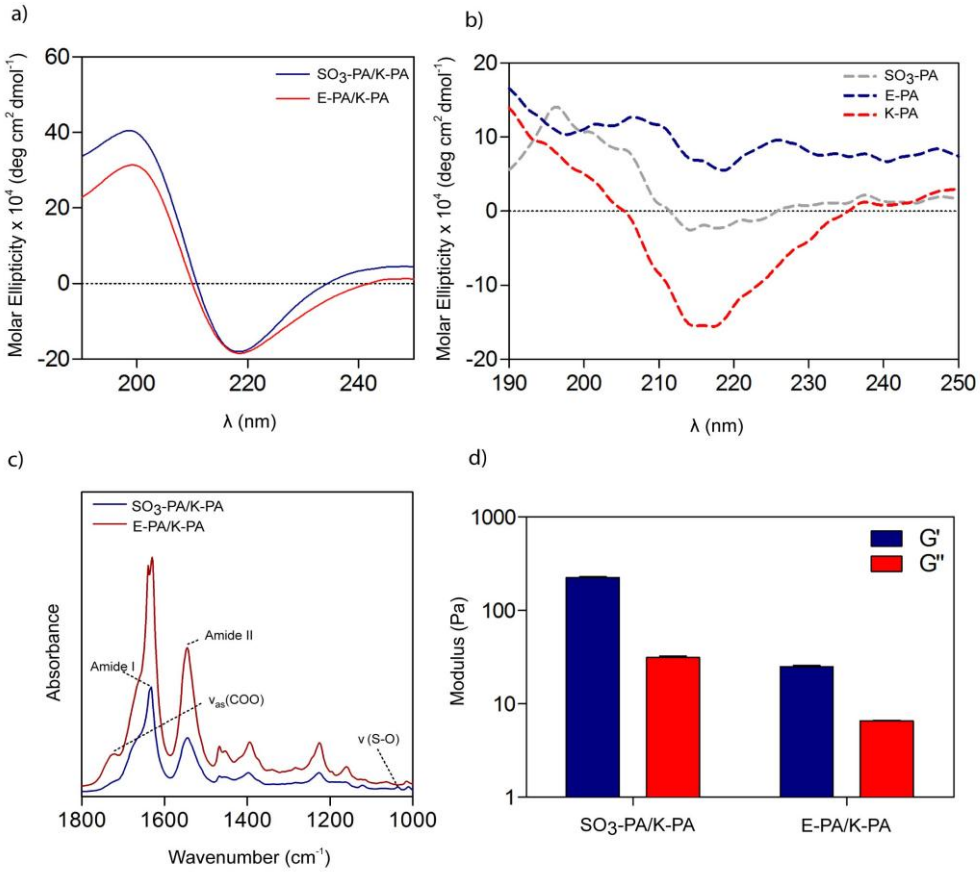

Figure 2.4 Circular dichroism of a) SO_3-PA/K-PA and E-PA/K-PA peptide nanofibers and b) SO_3-PA, K-PA and E-PA individually. c) FT-IR spectrum of SO_3-PA/K-PA and E-PA/K-PA peptide nanofibers. d) Rheology measurements of SO_3-PA/K-PA and E-PA/K-PA.

2.3.3.5 Oscillatory Rheology

Rheology experiment was applied to peptide nanofibers in order to indicate gel formation upon mixing oppositely charged peptide amphiphiles. Gel formation is defined in terms of storage modulus (G′) is higher than the loss modules (G″) where a shift from viscous liquid to gel form is taken place. In our system, the storage moduli of all samples were higher than the loss moduli which prove the gel formation. (Figure 2.4 d)

2.3.4 2-D Cell Culture on Peptide Nanofibers

2.3.4.1 Design of 2D Cell Culture Experiments

Glycosaminoglycan-mimetic PAs were coated onto tissue culture plates and coverslips to determine the effect of chemical groups on PAs to the cellular behaviors such as viability, spreading, proliferation and mineralization in two-dimensional cell culture. SO_3-PA/K-PA nanofibers were used to mimic sulfonated glycosaminoglycans and E-PA/K-PA nanofibers were used for unsulfonated glycosaminoglycans. As a control, uncoated tissue culture plates were used which are lacks of peptide nanofibers. Saos-2 cells are used in all *in vitro* experiments due to their osteoblast-like phenotypes and mineralization capacities.

2.3.4.2 Cell viability and morphology

Viability of osteoblast-like cells was assessed with Calcein-AM staining. Calcein-AM is a cell-permeable and nonfluorescent dye which is converted into fluorescent calcein upon acetoxymethyl ester hydrolysis by intracellular

esterases and gives green color. 3 days after incubation in growth medium, cells on glycosaminoglycan-mimetic peptide nanofibers and tissue culture plates were stained with Calcein to utilize their viabilities. Viability of osteoblast-like cells was similar on all sample types after 3 days of incubation. (Figure 2.5) This figure indicates that glycosaminoglycan-mimetic peptide nanofibers have not any toxic affect on cells and they provide biocompatible and biofriendly environments where cells can live. The morphology of cells on glycosaminoglycan-mimetic peptide nanofibers was observed by SEM. The morphology of cells on all samples was similar. Osteoblasts spread on all surfaces and attained their characteristic morphologies by the end of day 3. (Figure 2.5)

2.3.4.3 Proliferation

Cell proliferation was examined by each other day. At the beginning of the experiments, quantitative results revealed that equal number of cells were live 24 h after incubation on glycosaminoglycan-mimetic peptide nanofibers and TCP where none of the surfaces were completely covered with cells. On day 3, number of cells on both samples increased 4-fold with respect to the cell numbers of day 1 which indicates that cells duplicated every day. The number of cells on SO_3-PA/K-PA and TCP were 1.3 fold higher the cells on E-PA/K-PA at the end of day 3. On day 5, proliferation rates of cells were decreased around 0.74 fold on SO_3-PA/K-PA nanofibers and 0.78 fold on E-PA K-PA nanofibers.

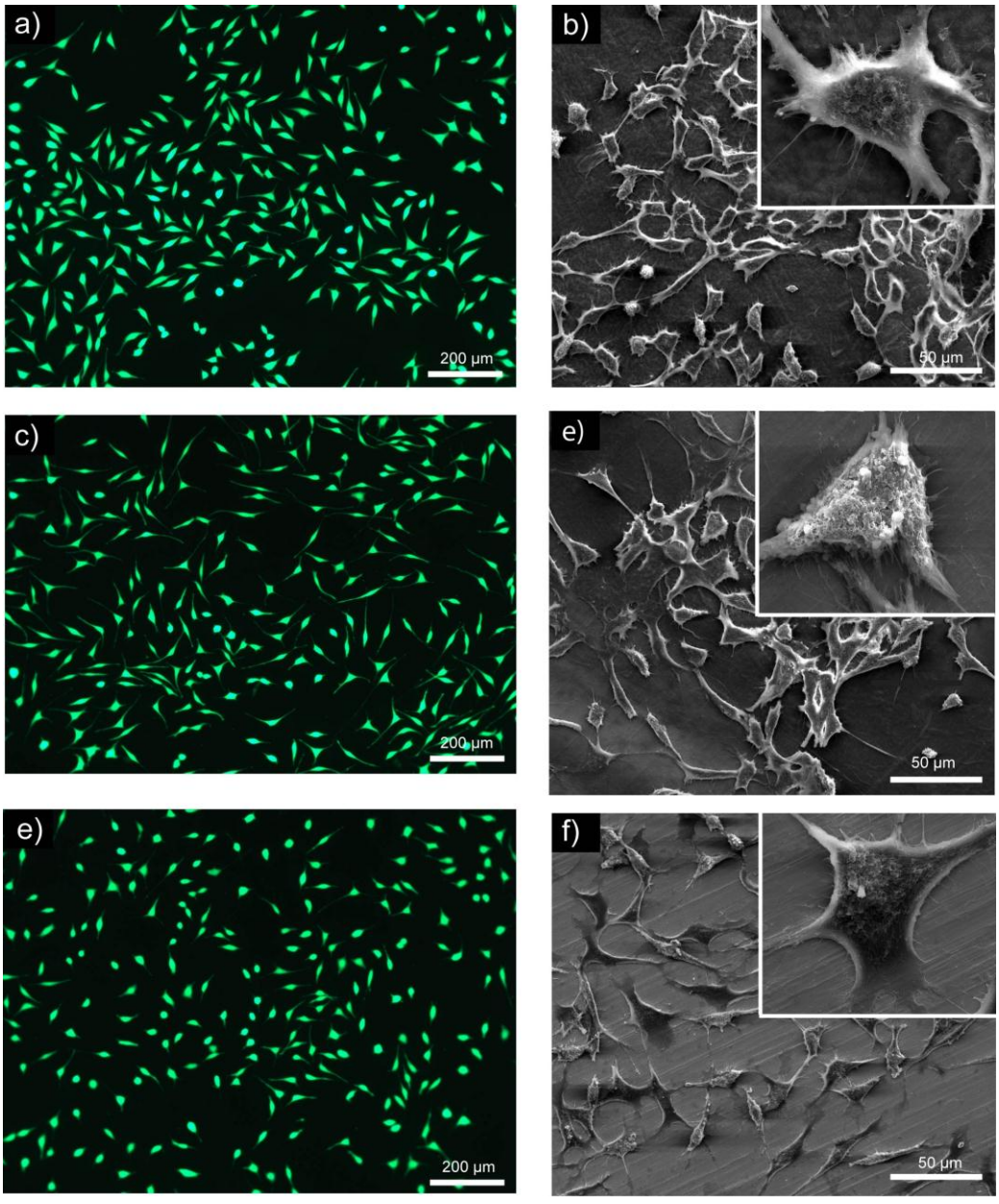

Figure 2.5 Viability and morphology of Saos-2 cells on glycosaminoglycan-mimetic peptide nanofibers after 3 days of incubation. SO_3-PA/K-PA (a-b), E-PA/K-PA (c-d) and tissue culture plate (e-f).

However, no change of proliferation rate was observed on TCP at the end of day 5. (Figure 2.6) Overall, osteoblastic cells proliferated on all samples over 5 days; however proliferation ratio decreased on GAG-mimetic peptide nanofibers after day 3 which could be explained with initiation of differentiation after certain confluency.[100] In fact, glycosaminoglycans can decrease the proliferation of osteoblasts and osteoblast-like cells as shown in previous experiments. [101]

2.3.4.4 BMP-2 Binding Assay

Binding of BMP-2 on glycosaminoglycan-mimetic peptide nanofibers was measured with ELISA. (Figure 2.7) 1 mM and 0.1 mM SO_3-PA/K-PA and E-PA/K-PA nanofibers were used for the experiment. After BMP-2 incubation on nanofibers, it was observed that binding of BMP-2 on SO_3-PA/K-PA was 1.33 fold higher than the binding of BMP-2 on E-PA/K-PA nanofibers when 100 ng/ml BMP-2 was used. The average optical density at this concentration is around 1.03 for SO_3-PA/K-PA and 0.77 for E-PA/K-PA nanofibers. Very low binding was observed on uncoated ELISA plates which average optical density is around 0.07 that indicates the BMP-2 binds to peptide nanofibers specifically. When amount of BMP-2 is decreased to 10 ng/ml, similar binding patterns were acquired on all samples. Most binding of BMP-2 was observed on SO_3-PA/K-PA nanofibers which is 3.3 folds higher than the binding on E-PA/K-PA nanofibers. The average optical density at this concentration is around 0.19 for SO_3-PA/K-PA and 0.06 for E-PA/K-PA nanofibers, whereas it is around 0.02 for uncoated samples.

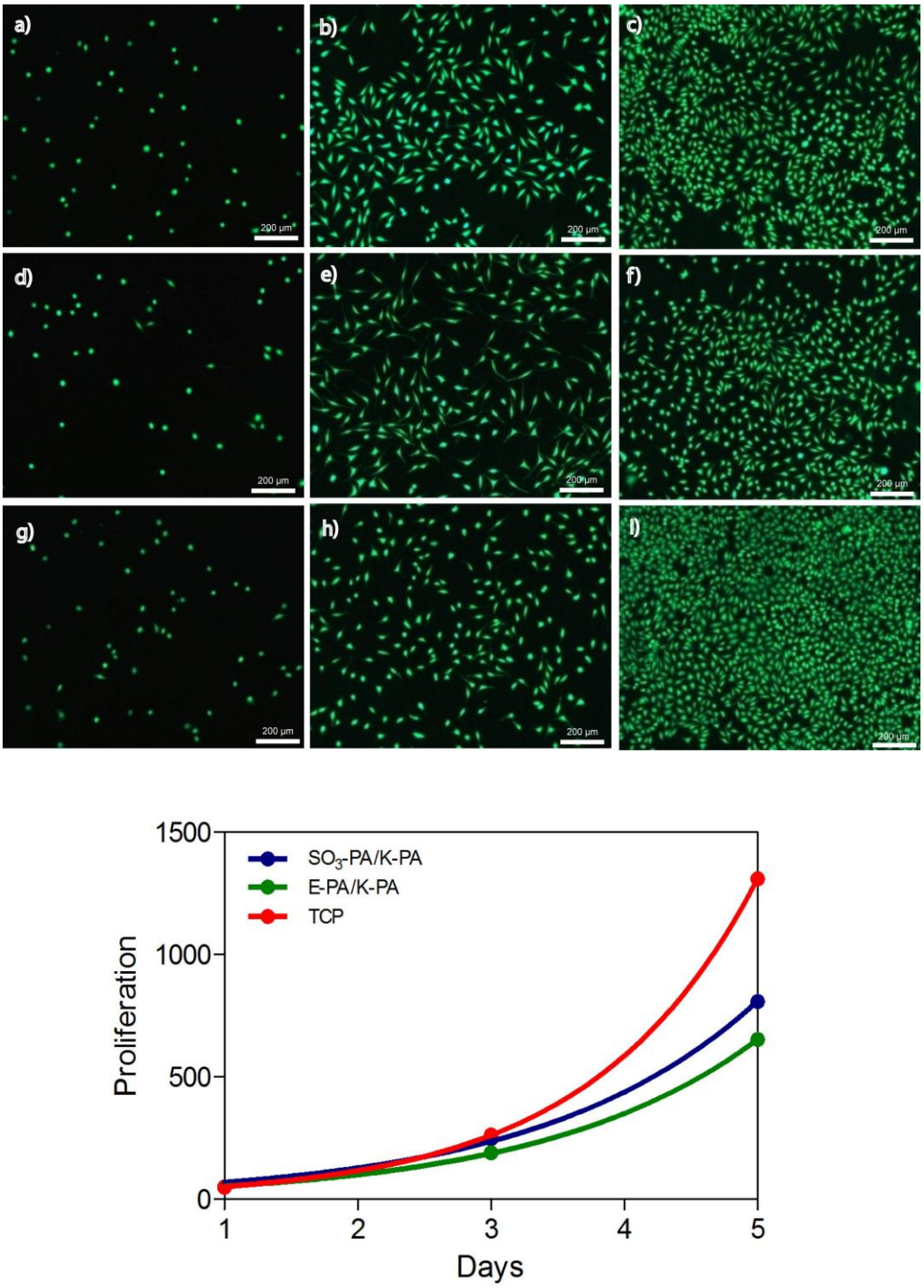

Figure 2.6 Proliferation of Saos-2 cells on glycosaminoglycan-mimetic peptide nanofibers over 5 days stained with Calcein. SO_3-PA/K-PA (a-c), E-PA/K-PA (d-f) and TCP (g-i) at day 1 (a,d,g), day 3 (b,e,h) and day 5 (c,f,i)

Sulfonation and negative charge density could be the critical parameters for more BMP-2 binding on SO_3-PA/K-PA nanofibers according to these results. Similar results were also obtained when 0.1 mM peptide nanofibers were used for binding. This result indicates that the concentration of peptide amphiphiles (0.1 mM) are enough to allow binding of 100 ng/mL BMP-2, in other words; peptide nanofibers were already saturated at this concentration. Lower PA concentration could be tested to see the effect of ligand (chemical groups on PAs) density on binding of BMP-2.

2.3.4.5 ALP Activity

ALP activity of osteoblast-likes cells was varying related to the samples where cells cultured on. (Figure 2.8) At day 1, significantly higher ALP activity was observed on SO_3-PA/K-PA and E-PA/K-PA as compared to the TCP surfaces. Addition of BMP-2 also increased the ALP activity of cells on glycosaminoglycan-mimetic peptide nanofibers about 2 folds for SO_3-PA/K-PA and 1.5 folds for E-PA/K-PA; however, no change in ALP activity was seen on TCP samples. At day 3, BMP-2 addition to the culture media did not alter the ALP activity of cells on all samples, however there is still significant difference between ALP activity of cells on glycosaminoglycan-mimetic peptide nanofibers and the cells on TCP. ALP activity of osteoblast-like cells indicated similar trend for all sample types such that it reached maximum on day 7 and decreased afterwards. On day 7, maximum ALP activity of osteoblast-like cells was observed on SO_3-PA/K-PA nanofibers and BMP-2 addition increased ALP activity significantly.

a)

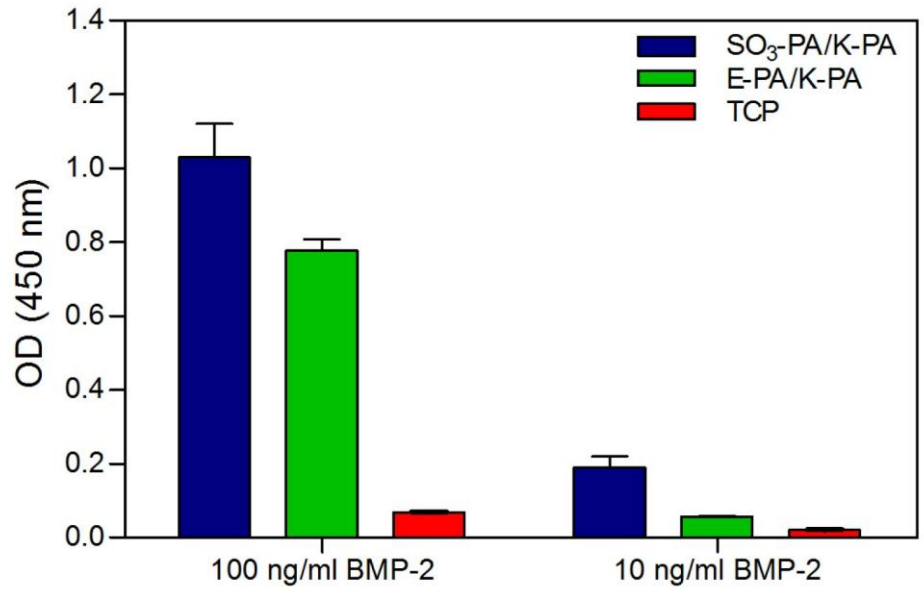

b)

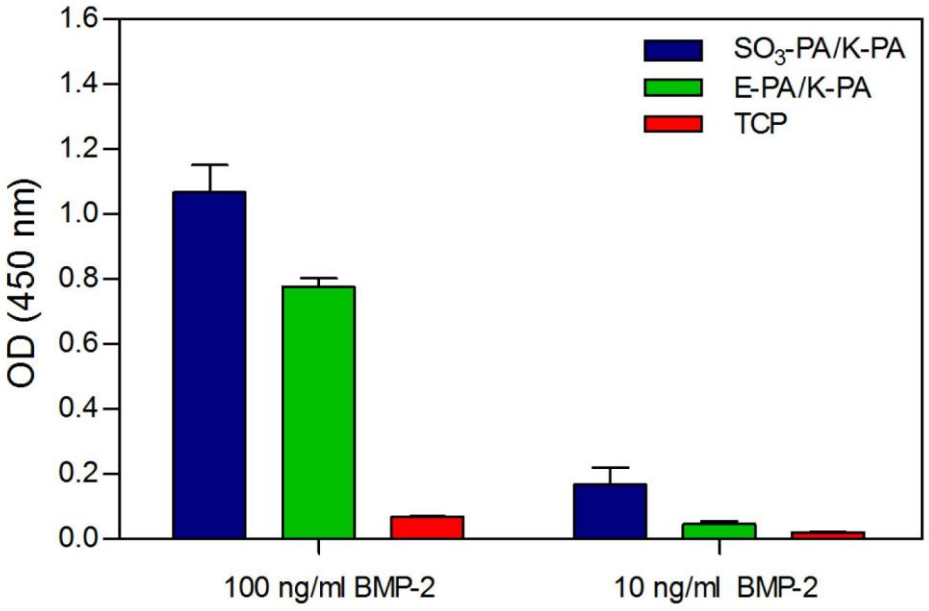

Figure 2.7 BMP-2 binding on glycosaminoglycan-mimetic peptide nanofibers analyzed by ELISA assay.

ALP activity of cells on these nanofibers was significantly higher compared to all other sample types both in the presence and absence of BMP-2. ALP activity of cells on E-PA/K-PA nanofibers also increased significantly upon BMP-2 addition and was significantly higher with respect to the TCP samples both in the presence and absence of BMP-2. However, no change was observed in ALP activity of TCP samples according to the BMP-2 addition although ALP activity of cells on these surfaces increased in comparison to day 1 and day 3 samples. On day 10, ALP activity of cells decreased in all samples but the significant difference between glycosaminoglycan-mimetic peptide nanofibers and TCP continued in both BMP-2 dependent conditions. Moreover, only SO_3-PA/K-PA nanofibers showed higher ALP activity in the presence of BMP-2 compared to non-BMP-2 treated samples.

Alkaline phosphatase (ALP) is an enzyme which is responsible for hydrolysis of inorganic pyrophosphate to produce inorganic phosphate, which is used in mineralization process. [102] The activity of this enzyme is believed to be upregulated in early stages of mineralization to provide a large inorganic phosphate source from which hydroxyapatite can be mineralized. [103] After a certain point where enough phosphate is produced, ALP is no longer needed and the enzymatic activity drops before the formation of mature mineralized matrix. The maximum ALP activity observed on day 7 and the decrease through day 10 indicates initiation of mineralization for all samples. When ALP activity over 10 days was analyzed, we observe that ALP activity of cells was always higher on glycosaminoglycan-mimetic peptide nanofibers in comparison to TCP.

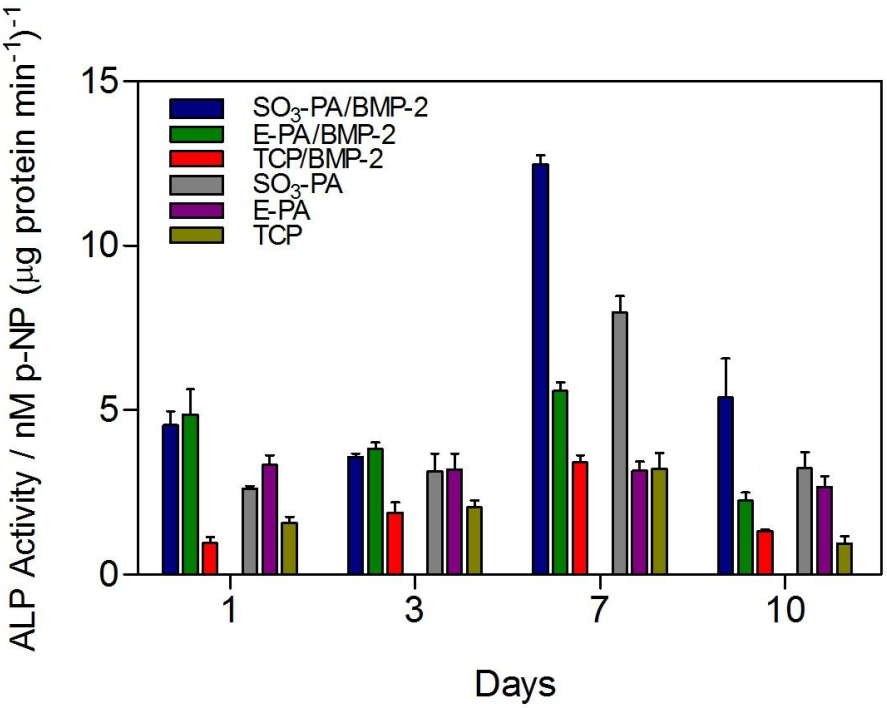

Figure 2.8 Effect of glycosaminoglycan-mimetic peptide nanofibers on alkaline phosphatase activity of Saos-2 cells on days 1, 3, 7 and 10 in the presence (100 ng/mL) or absence of BMP-2.

Moreover, presence of BMP-2 increased ALP activity especially on SO_3-PA/K-PA nanofibers on almost all days that we have tested and slightly increased that of E-PA/K-PA on day 7, whereas no significant difference was observed for TCP samples in the presence of BMP-2 on any of the days that were analyzed. These results show that glycosaminoglycan-mimetic peptide nanofibers could be responsible for the increase of ALP activity upon BMP-2 binding and its presentation to cell surface receptors. [104]

2.3.4.6 Mineralization

Osteoblasts undergo *in vitro* mineralization by forming mineralized bone nodules which are about 35-100 μm in diameter and consist of three-dimensional cell aggregates and collagen ECM. In our system, mineralized matrix formation was observed with Alizarin Red staining. (Figure 2.9) Alizarin Red- S is a commonly used method where Alizarin Red- S selectively binds to calcium in mineralized matrix of bone cells at a ratio of 1:2. [105] Staining of calcium in the mineralized matrix was observed under light microscopy. 14 days after incubation in osteogenic medium in the presence or absence of BMP-2, calcium deposition was assessed. Osteoblasts formed mineralized bone nodules on glycosaminoglycan-mimetic peptide nanofibers upon migration and 3-D aggregate formation which contains cells and fibrous ECM [106-108]; however no mineralized nodule formation was seen in TCP samples both in the presence or absence of BMP-2. Mineralized nodules seen on SO_3-PA/K-PA nanofibers were higher in number with respect to the nodules on E-PA/K-PA nanofibers.

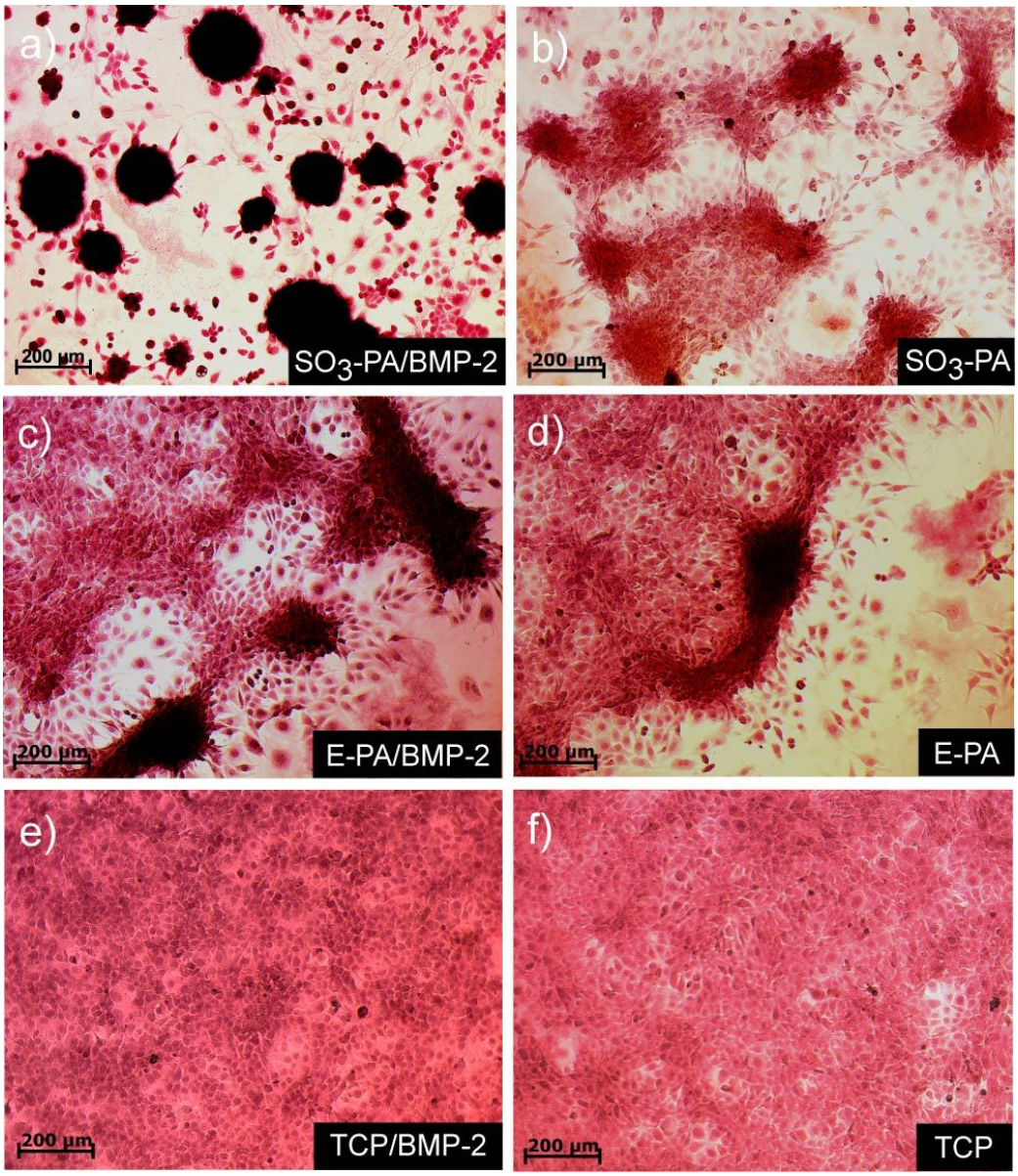

Figure 2.9 Alizarin Red staining of mineralized *in vitro* bone-like nodules on glycosaminoglycan-mimetic peptide nanofibers on day 14 in the presence (a, c and e) or absence (b, d and f) of BMP-2. SO_3-PA/K-PA (a-b), E-PA/K-PA (c-d) and bare surface (e-f).

Mineralized nodules were also qualitatively larger and denser in the presence of BMP-2.

2.3.4.7 Bone Nodule Formation

In our system, bone nodule formation was observed on glycosaminoglycan-mimetic peptide nanofibers by using SEM. (Figure 2.10) At the end of day 14, nodules were present only on SO_3-PA/K-PA and E-PA/K-PA nanofibers; however, no nodule formation was seen on uncoated surfaces. These nodules were around 100-200 μm in diameter where collagen like fibrillar ECM and spherical minerals accumulated on top of the 3-D cell aggregates. These structures were clearly seen especially on SO_3-PA/K-PA nanofibers, and also on E-PA/K-PA nanofibers. To determine the chemical composition of samples, EDAX spectroscopy was used at 80x magnification. EDAX spectra obtained from these samples revealed that carbon (C), nitrogen (N) and oxygen (O) specific peaks were detected on both SO_3-PA/K-PA and E-PA/K-PA nanofibers due to peptide nanofibers. However, we detected calcium (Ca) and phosphorus (P) peaks predominantly on SO_3-PA/K-PA nanofibers. Ca and P were also present on E-PA/K-PA nanofibers, while their abundance was lower compared to SO_3-PA/K-PA nanofibers. Uncoated stainless steel surfaces showed iron (Fe) and nickel (Ni) peaks as the surface was not coated with nanofibers, and there was very low detectable amount of Ca and P on these surfaces.

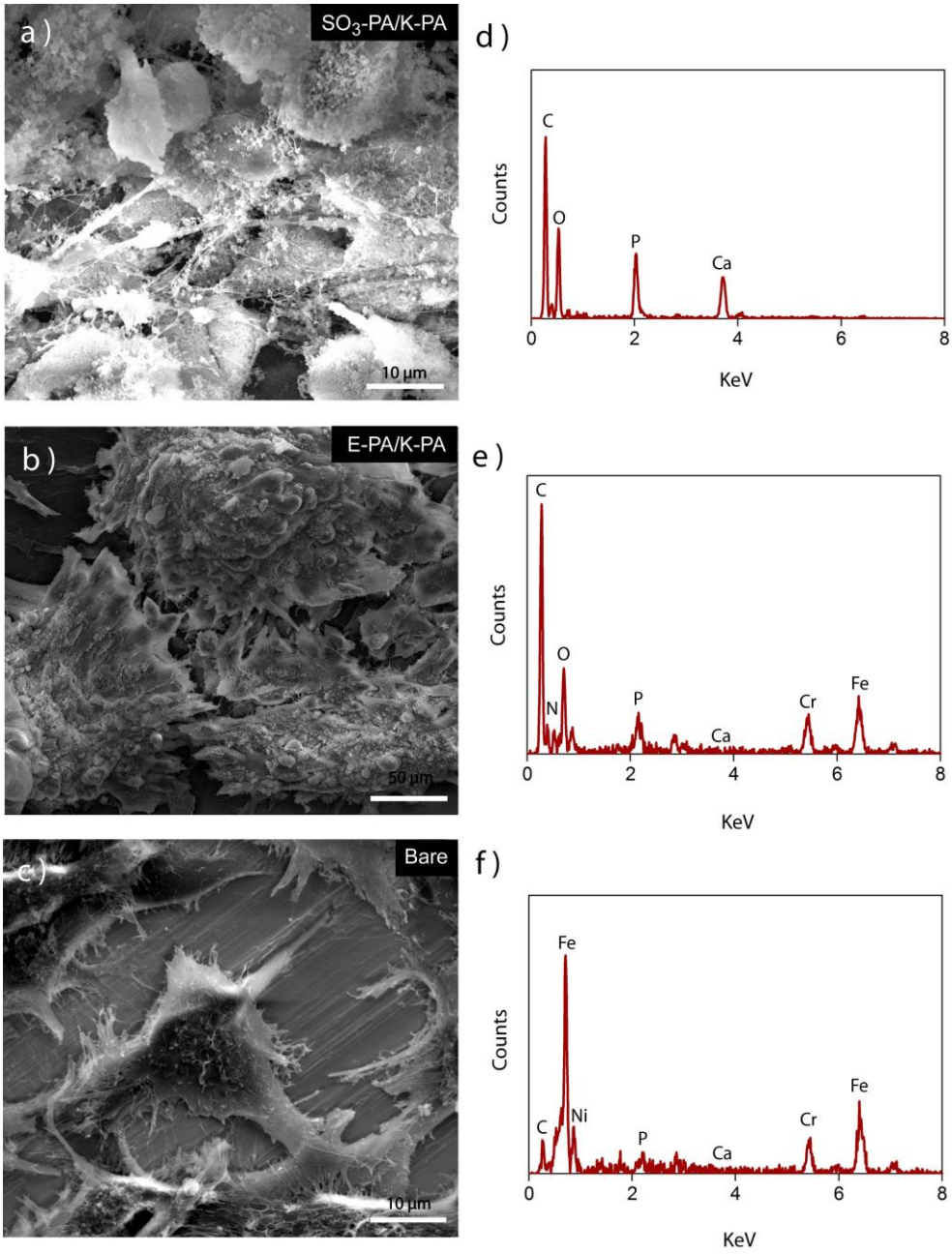

Figure 2.10 SEM images and EDAX analysis of mineralized bone-like nodules on glycosaminoglycan-mimetic peptide nanofibers. SO_3-PA/K-PA (a-d), E-PA/K-PA (b-e) and bare surface (c-f).

2.5 Conclusion

Glycosaminoglycan-mimetic peptide nanofibers were designed to mimic the structure of glycosaminoglycans found in the extracellular matrix which have great importance in bone regeneration and mineralization process. They were decorated with carboxyl, hydroxyl and sulfonate groups that are abundant on the glycosaminoglycans found in bone. In this way, binding of BMP-2 on glycosaminoglycan-mimetic peptide nanofibers was triggered which provides osteoinductive characteristics to peptide nanofibers. Glycosaminoglycan-mimetic peptide nanofibers provided biocompatible and adapted microenvironment for osteoblastic cell growth, spreading and proliferation. Furthermore, osteoblast-like cells cultured on these nanofibers exhibited enhanced osteogenic activity. It was observed that alkaline phosphatase activity and calcium deposition which are the main indicators of bone-like mineralization were enhanced on these nanofibers. More importantly, osteogenic activity of cells was boosted in the presence of BMP-2 on sulfonated peptide nanofibers. This work indicates glycosaminoglycan-mimetic peptide nanofibers are osteoinductive materials which have potential for bone tissue engineering applications by using either directly or as a carrier system together with growth factors.

Chapter 3

Surface-Adhesive and Osteogenic Self-Assembled Peptide Nanofibers for Titanium Implant Biofunctionalization

This work was partially published in the following publication:

Kocabey, S.; Ceylan, H.; Tekinay, A.B.; Guler, M.O.; Surface-adhesive and osteogenic self-assembled peptide nanofibers for bioinspired functionalization of titanium surfaces. ***Soft Matter***, 2012, 8, 3929-3937.

3.1 Introduction

Titanium-based materials are widely used as orthopedic and dental implants because of their mechanical properties and biological inertness. [109-110] A major concern with titanium implants is integration into the existing tissue. When bone cells cannot adhere to the surface of the implanted material, the implant cannot be integrated and will eventually detach from the body in the long term. Guiding cellular behaviors such as adhesion, viability, proliferation, migration, and differentiation of cells that are in contact with the implant has been a critical concern for enhancing osseointegration event. In order to overcome tissue integration problems, most of the past and current research has concentrated on modification of bone implants' surface properties by increasing roughness and altering surface chemistry, mostly coating surface with an oxide layer or immobilizing hydroxyapatite. [111-115] On the other hand,

modification of implant surfaces with biologically active cues to mimic extracellular matrix has recently emerged as a promising approach to enhance osseointegration. [116-120] The ECM constituents regulate cellular behaviors in natural cellular microenvironment by providing cells with spatially and temporally controlled bioactive signals.

The ability of self-assembled peptide amphiphile nanofibers to mimic ECM has been under intensive research in recent years, since such biodegradable nano-scale matrices created by these nanofibers closely matches to that of the native ECM. Moreover, the flexibility in their design allows a wide range of bioactive sequence conjugation, which has been shown to be efficiently presented to the cells in order to promote cellular adhesion, proliferation, and differentiation both in *in vitro* and *in vivo* environments. [23, 121-122] These characteristics are solely controlled through the design of building blocks that form the nanofibers.[52, 111] These nanofibers were capable of mimicking the adhesion strategy of mussels, so that the nanofibers could be conveniently immobilized onto the titanium surface, and presenting an osteoblast cell-specific adhesion epitope, KRSR.

Promoting osteoblast adhesion and survival on titanium in a selective manner is a challenging task. Rapid and selective adhesion and growth of osteoblasts are critical because delayed healing can cause fibroblast-mediated scar tissue formation leading to tissue softening around the implant and further revision surgeries. [123-126] On the other hand, the KRSR peptide sequence, which binds to transmembrane proteoglycans, was shown to promote selective

adhesion of osteoblasts, while, at the same time, inhibiting the adhesion of fibroblasts. [54, 127-128]

Although novel soft materials as bioactive interface between the implant and the tissue to enhance compatibility and durability of the implant is a developing alternative, most of the available materials suffer from inefficiency to be stable on the implant surface in aqueous environment. Functionalization of the implant surface such as with biotin-streptavidin and nitriloacetic acid-histidine interactions, provide a reversible adhesion platform under controlled conditions, however, these techniques are weak in terms of adhesion strength and require surface preparation prior to immobilization. Covalent attachment techniques such as N-hydroxysuccinimide (NHS)-ethyl (dimethylaminopropyl) carbodiimide (EDC) coupling ensure strong surface binding and thus offer a wider range of applications. Nevertheless, in addition to the persisting need for surface preparation, these systems are mostly susceptible to hydrolysis that lowers the efficiency of immobilization and their degradation products may cause biocompatibility issues. [129-131]

To overcome disadvantages of the currently available adhesive methods for medical applications, a sessile organism, mussel, offers a valuable strategy that allows adhesion to inorganic and organic surfaces in the presence of water. Mussels adhere to surfaces via special adhesive proteins that are highly enriched with 3,4-dihydroxy-L-phenyl alanine (Dopa), which forms strong bonds with hydrophilic surfaces and complexes with metal ions and metal oxides. [132] Thus, conjugating Dopa to synthetic materials attracts growing attention not

only because it can operate under aqueous conditions without requiring any surface preparation but also because it is fully biocompatible. [133] In terms of adhesion strength, Dopa adhesion displays a covalent character whilst it is resistant to hydrolysis and is fully reversible.[134] Lee *et al.* measured dissociation force between Dopa and TiO_2 as 805 pN, which is closer to the dissociation force of a typical carbon-silicon covalent bond (2000 pN) and much higher than the dissociation force of hydrogen bonds that hold DNA double helix intact (10-20 pN), indicating the strength of the adhesion formed between Dopa and TiO_2. [134-135]

This chapter discusses a study of adhesive and osteogenic self-assembled peptide nanofibers designed to investigate functionalization of titanium implants and effect of these nanofibers on osteogenic activity. Peptide amphiphiles used in this study provide an interface through metal adhesive Dopa molecule and osteoblast adhesion sequence, KRSR. We describe below the design and characterization of adhesive and osteogenic peptide nanofibers, surface characteristics of peptide nanofiber coated titanium and the affect of these nanofibers on osteogenic cell behaviors such as adhesion, viability, and mineralization.

3.2 Experimental

3.2.1 Synthesis of Surface-Adhesive and Osteogenic Peptide Amphiphiles

Surface-adhesive and osteogenic peptide amphiphile molecules were synthesized by solid phase peptide synthesis using standard Fmoc chemistry. Peptide synthesis was performed manually on a 0.25 or 0.5 mmole scale using a 50 ml fritted vessel on a wrist action shaker. Peptide molecules were synthesized on Rink Amide Resin or Fmoc-Glu(OtBu)-Wang resin by coupling from their C-terminal ends. In each coupling, 20% Piperidine/DMF (N,N dimethylformamide) was used to remove Fmoc protection groups for 20 min. After each reaction, washing was performed with DMF, DCM and DMF respectively. All aminoacid couplings were performed by using 2:1.95:3 equivalents of aminoacids, HBTU and DIEA for 2 hr. To block unreacted amine groups irreversibly in the reaction, %10 acetic anhydride/DMF solution was added on resin. Coupling reactions were repeated until addition of alkyl tails. After addition of the last reagent, peptide cleavage from resin and deprotection were performed using 95:2.5:2.5 TFA:TIS:H_2O for 3 h on shaker. In order to remove unwanted TFA and DCM from peptide solution, rotary evaporation was carried out at 40 ºC for less than 20 min. After evaporation, ice cold diethylether was added into round bottom flask and incubated at -20 °C overnight. Following day, the precipitated peptide was collected after centrifugation and dissolved in ultra-pure water. Dissolved peptide solution was frozen at -80 °C. Finally, freeze drying in lyophilizer was performed on frozen peptide solution.

3.2.2 Mass Spectrometry and HPLC Purification

To characterize synthesized peptide amphiphiles, a quadruple time of flight (Q-TOF) mass spectrometer with electrospray ionization (ESI) source equipped with a reverse-phase analytical high performance liquid chromatography (HPLC) was used. Agilent Zorbax SB-C8 4.6 mm x 100 mm column was used for positively charged peptide molecules and Agilent Zorbax Extend-C18 2.1 x 50 mm column was used for negatively charged peptide molecules. %0.1 formic acid/water and %0.1 formic acid/acetonitrile were used for positively charged peptide molecules as inorganic and organic solvents. For negatively charged peptide molecules %0.1 NH_4OH/water and %0.1 NH_4OH /acetonitrile were used. Reverse phase Prep-HPLC was used for purification of peptide amphiphiles. Zorbax SB-C8 21.2 x 150 mm column for positively charged peptide molecules and Zorbax Extend-C18 21.2 x 150 mm column for negatively charged peptide molecules were used in mobile phase. A gradient of water (0.1% TFA and 0.1% NH_4OH) and acetonitrile (0.1% TFA and 0.1% NH_4OH) was used. Furthermore, positively-charged peptide amphiphiles were treated with 0.1 M HCl solution in order to remove residual TFA at the end.

3.2.3 PA Characterizations

KRSR-PA/Dopa-PA nanofibers were formed by mixing KRSR-PA and Dopa-PA at 1:3 ratios, respectively, which stabilizes all net charges at pH 7.4. For the same reason, KRSR-PA and E-PA were mixed at 2:3 ratios, respectively, to form KRSR-PA/E-PA, and K-PA and Dopa-PA were mixed at 1:1 ratios to form K-PA/Dopa-PA nanofibers. SEM samples were prepared by mixing KRSR-

PA/Dopa-PA at 1 mM and 3 mM concentrations, respectively, and then by critical-point drying following ethanol exchange. The samples were coated with 4-5 nm Au-Pd before imaging. Scanning transmission electron microscopy (STEM) images were acquired with FEI Tecnai G2 F30 TEM at 300 kV. Samples for STEM were prepared by mixing 1 mM KRSR-PA and Dopa-PA at 1:3 ratio, respectively, on a 200-mesh carbon TEM grid for 1 min followed by 2 wt% uranyl-acetate staining for 30 s and drying immediately under nitrogen gas. The samples for circular dichroism (Jasco J-815) were prepared by mixing KRSR-PA and Dopa-PA at 1 x 10^{-5} and 3 x 10^{-5} M concentrations, respectively. Zeta potential measurements (Malvern Zeta-ZS) of individual PA solutions or their mixtures were performed at the given ratios above at concentrations in the order of 10^{-4} M. Frequency sweep rheology measurements (Anton Paar Physica RM301) were performed using PA mixtures at 10^{-3} M concentration.

3.2.4 Surface Characterizations

Adsorption of Dopa-PA and KRSR-PA on titanium surface was analyzed by X-Ray Photoelectron Spectroscopy (XPS), Attenuated Total Internal Reflectance Fourier transform infrared spectroscopy (ATR-FT-IR), Scanning Electron Microscope (SEM), contact angle measurements (OCA 30 Dataphysics), and optical profilometer (Zygo New view 7200). Surface binding tests of nanofibers onto surfaces were carried out against water competition. 1 mM KRSR-PA and Dopa-PA solutions were mixed on sterilized titanium at 1:3 ratios. Control for Dopa was designed using KRSR-PA and E-PA nanofibers, which were mixed at

2:3 ratios, respectively. The samples were kept in a humidified environment for 24 h at room temperature to prevent evaporation. Then, substrates were rinsed in water for 30 min and dried at 37 °C for a further 24 h. In a different approach, we tested retention of the coating in various solvents by slowly drying for a couple of days. Then, the substrates were washed in ethanol, 2-propanol, acetone, cell culture medium (10% FBS containing DMEM), and PBS coupled with ultrasound sonication up to 2 h. To characterize the chemical composition and molecular structure of the nanofiber network formed on the surface upon drying; XPS and FT-IR spectra measurements were taken on the surface. A Thermo Scientific XPS spectrometer with Al-Kamonochromatic (100-400 eV range) X-ray source and ultrahigh vacuum (~10^{-9} Torr) was used to identify the chemical composition of the surface with high resolution scans. Results were acquired from at least three different locations on the surface. A VORTEX 70 Fourier transform infrared spectrometer equipped with liquid nitrogen-cooled MCT detector was utilized to identify the FT-IR spectrum of the surface by using germanium ATR objective with spectrum range between 4000 and 400 cm^{-1}. As in XPS measurements, results were acquired from at least three different locations of the surface.

Samples for optical profilometer were coated with 5 nm Au-Pd before measurement. SEM samples were prepared by ethanol gradient and critical point drying (Tourismis Autosamdri®-815B) followed by 4-5 nm Au-Pd coating.

3.2.5 Cell Culture

Saos-2 (human osteosarcoma cell line, ATCC^{R} HTB-85^{TM}), MC-3T3 (mouse pre-osteoblastic cells) and HGF (Human gingival fibroblast cells) were used in adhesion, spreading, viability and proliferation experiments. HGF cells were isolated and characterized as described and were kindly provided as a gift from Prof. Dr. A.U. Ural of GATA, Ankara, Turkey.[141] All cells were cultured in 75 cm^2 cell culture flasks containing Dulbecco's Modified Eagle Serum (DMEM) supplemented with 10% Fetal Bovine Serum (FBS), 1% Penicillin/Streptomycin and 2 mM L-Glutamine. Cells were grown at 37 ºC in a humidified atmosphere supplied with 5% CO_2. All cell experiments were carried out after 90-100% confluency was reached and cells were diluted 1/3 and 1/4 for subculture.

Saos-2 cells were used in ALP activity and mineralization experiments. Cells were seeded on titanium disks in 24 well plates at a density of 10^4 cells/cm^2 in DMEM medium supplemented with 10% FBS. After reaching confluency, maintenance medium was replaced with fresh osteogenic medium that contains 10 mM β-Glycerophosphate, 0.2 mM Ascorbic acid and 100 nM Dexamethasone in addition to the maintenance medium.

3.2.6 Cell Adhesion & Spreading

Adhesion and spreading experiments of Saos-2, HGF and MC-3T3 cells were analyzed on PA-coated and bare titanium surfaces after 1 h of incubation. Prior to cell seeding, cells were incubated in serum free DMEM medium supplemented with 4 mg/ml BSA and 50 µg/ml cyclohexamide for 1 h. Then,

cells were seeded on PA-coated/bare titanium surfaces in serum free DMEM medium at 1.5 x 10^4 cells/cm^2 density. 1 h after incubation, cells were rinsed with PBS once to get rid of unbound cells. Then, they were stained with 1 mM Calcein AM and cell adhesion was quantified by counting number of live cells in images taken under fluorescent microscope. Random images were taken from 10 independent regions on 1 cm^2 titanium surfaces (60 images/6 samples) and relative cell adhesion was determined by normalizing counted cells to the cells on bare titanium surfaces. For spreading, cell samples were either fixed with 3.7% formaldehyde followed by 10 min Triton X-100 permeabilization and TRITC-conjugated phalloidin treatment (for confocal microscopy) or 2% gluteraldehyde/PBS followed by post fixation with osmium tetroxide (for SEM imaging).

3.2.7 Cell Viability

Viability of Saos-2, HGF and MC-3T3 cells were analyzed on PA-coated and bare titanium surfaces after 24 h and 48 h of incubation respectively. Cells were seeded on PA-coated/bare titanium surfaces in DMEM medium supplemented with 10% FBS, 2 mM L-glutamine and 1% penicillin/streptomycin at 1.5 x 10^4 cells/cm^2 density. Cells were rinsed and stained with 1 mM Calcein AM after 24 h and 48 h of incubation. Viability of cells was quantified by counting number of live cells in images taken under fluorescent microscope. The total number of cells in each sample was normalized to the number of cells on bare titanium surfaces to obtain relative cell viability.

3.2.8 Alkaline Phosphatase Activity Assay

Saos-2 cells were collected at predetermined time points; 1, 3, 5 and 7 days after osteogenic medium replacement. Medium of cells was discarded and cells were rinsed with PBS once and then lyzed using 300 µl M-PER Protein Extraction Buffer (contains 5% protease inhibitor)/well on shaker for 20 min. Subsequently, lyzed cells were collected and centrifuged at 14000 g for 10 min and supernatants were transferred into chilled eppendorf tubes. 50 µl of supernatants were incubated with 150 µl of p-nitophenyl phosphate solution in a 96 well plate. ALP enzymatic activity was measured as conversion of p-nitophenyl phosphate to p-nitrophenol at 405 nm absorbance wavelength. The readings of samples acquired from microplate reader were compared with the readings of standard solutions of p-nitrophenol which were prepared by serial dilutions. Final ALP activity was presented as the ratio of produced p-nitrophenol to the extracted protein amount from cell lyzate at determined time point (min).

3.2.9 Alizarin Red-S Staining and Calcium Quantification

Saos-2 cells were collected at selected time intervals, 14 and 21 days after osteogenic medium replacement. Medium of cells was discarded and cells were fixed with ice cold ethanol (70%) for 1 hr and then rinsed twice with distilled water for 5-10 min each. Then, cells were stained with 40 mM Alizarin Red-S (pH 4.2) for 20 min at room temperature on shaker. Stained cells were then rinsed with distilled water for 4-5 times to get rid of non-specific Alizarin Red-S stain. Subsequently, to quantify Ca^{+2} concentration destaining procedure was

applied by using 10% (w/v) cetylpyridinium chloride in 10 mM Na_3PO_4 (pH 7). Finally, Alizarin Red-S concentration was measured at 562 nm absorbance wavelength by using Alizarin-Red S standards in the same solution. Ca^{+2} concentration was determined according to the equation that 1 mole AR-S binds to 2 moles of Ca^{+2} in the solution. [105]

3.3 Results and Discussion

3.3.1 Design and synthesis of Surface-Adhesive and Osteogenic PAs

Two different peptide amphiphile molecules were designed and synthesized by solid phase peptide synthesis to form nanofibers and to generate an osteoconductive surface where peptide nanofibers strongly adhered to the titanium surface and had osteogenic properties. For this purpose, Dopa-PA (Lauryl-VVAGE-Dopa-Am) was designed for titanium functionalization and KRSR-PA (Lauryl-VVAGKRSR-Am) was designed to promote osteogenic activity. These oppositely charged molecules self-assemble to form a nanofibrous network at physiological pH. To investigate the benefit of Dopa residue on the PA molecule, a PA molecule (E-PA) without Dopa residue (Lauryl-VVAGE) was synthesized. The utility of KRSR peptide in the PA construct was also tested by using a PA molecule (K-PA) that lacked the KRSR sequence but retained the rest of the peptide sequence (Lauryl-VVAGK-Am). (Figure 3.1)

3.3.2 Mass Spectrometry and HPLC Purification

To verify synthesized peptide amphiphiles qTOF-LCMS was performed. Expected masses were obtained for all PA molecules which were 1081 for KRSR-PA, 833 for Dopa-PA, 653 for E-PA and 651 for K-PA. (Figure 2.2) According to results obtained from LC-MS, preparative-HPLC was applied to peptide samples to get rid of impurities and peptide amphiphiles with 90% purity were obtained.

3.3.3 Self-assembly and Characterization of Peptide Amphiphiles

To visualize nanofiber formation upon mixing KRSR-PA and Dopa-PA, we performed SEM and TEM imaging. (Figure 3.3) Nanofibrous and porous network was formed through self-assembly of KRSR-PA and Dopa-PA at pH 7.4. To reveal the secondary structure of peptide nanofibers, we performed circular dichroism experiment (Figure 3.4 b). The chiral absorbance at 218 nm indicates β-sheet formation in KRSR-PA/Dopa-PA nanofibers and homogenous distribution of the building blocks within the nanofibers. Neither Dopa-PA nor KRSR-PA formed an organized structure by themselves in solution at pH 7.4. However, upon mixing, they predominantly formed β-sheet structures which indicate β-sheet-driven nanofiber formation. [99] Rheology measurements were performed to reveal mechanical properties of the nanofibrous hydrogels. Rheology results confirmed that a soft network was formed upon mixing KRSR-PA and Dopa-PA at pH 7.4 that was stabilized by physical entanglements of nanofibers, as in native ECM (Figure 3.4 a). To further verify the self-assembly process, zeta potential measurements were performed.

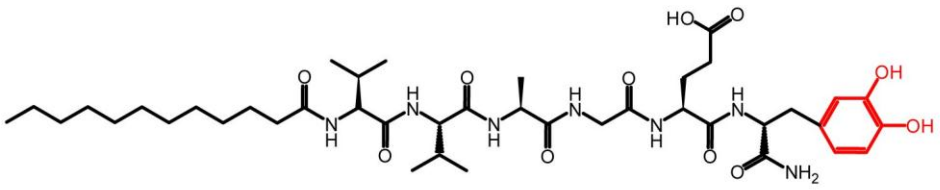

Dopa-PA

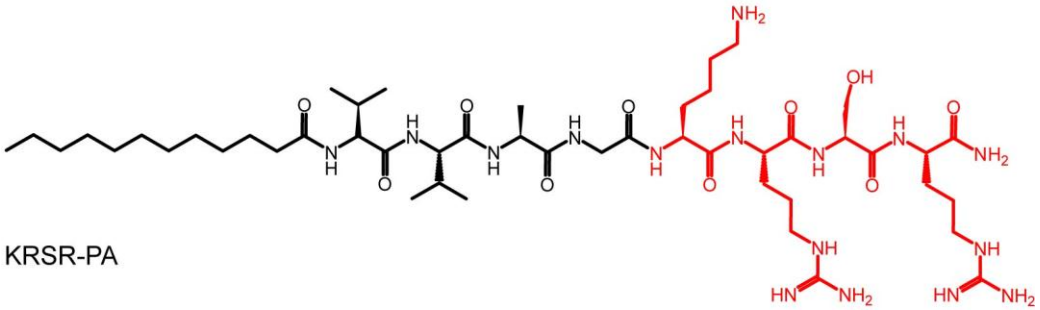

KRSR-PA

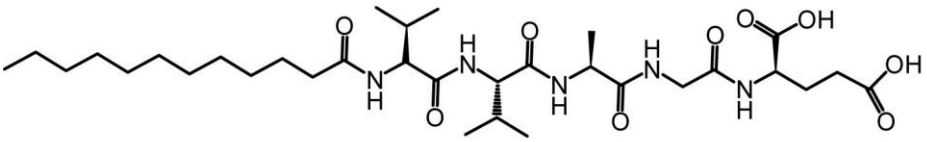

E-PA

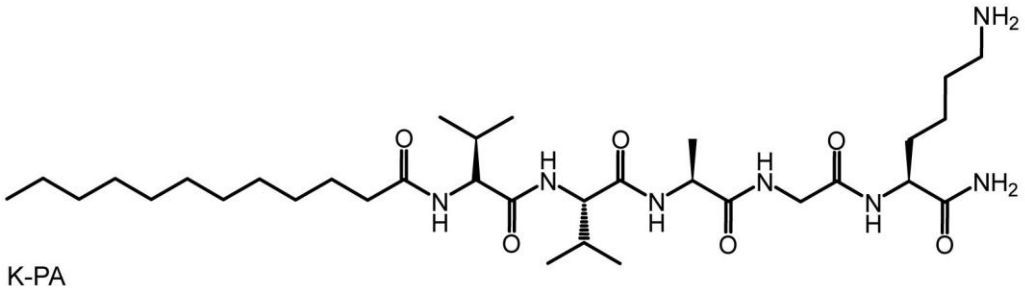

K-PA

Figure 3.1 Chemical structures of the peptide amphiphile molecules designed for functionalization of titanium surfaces.

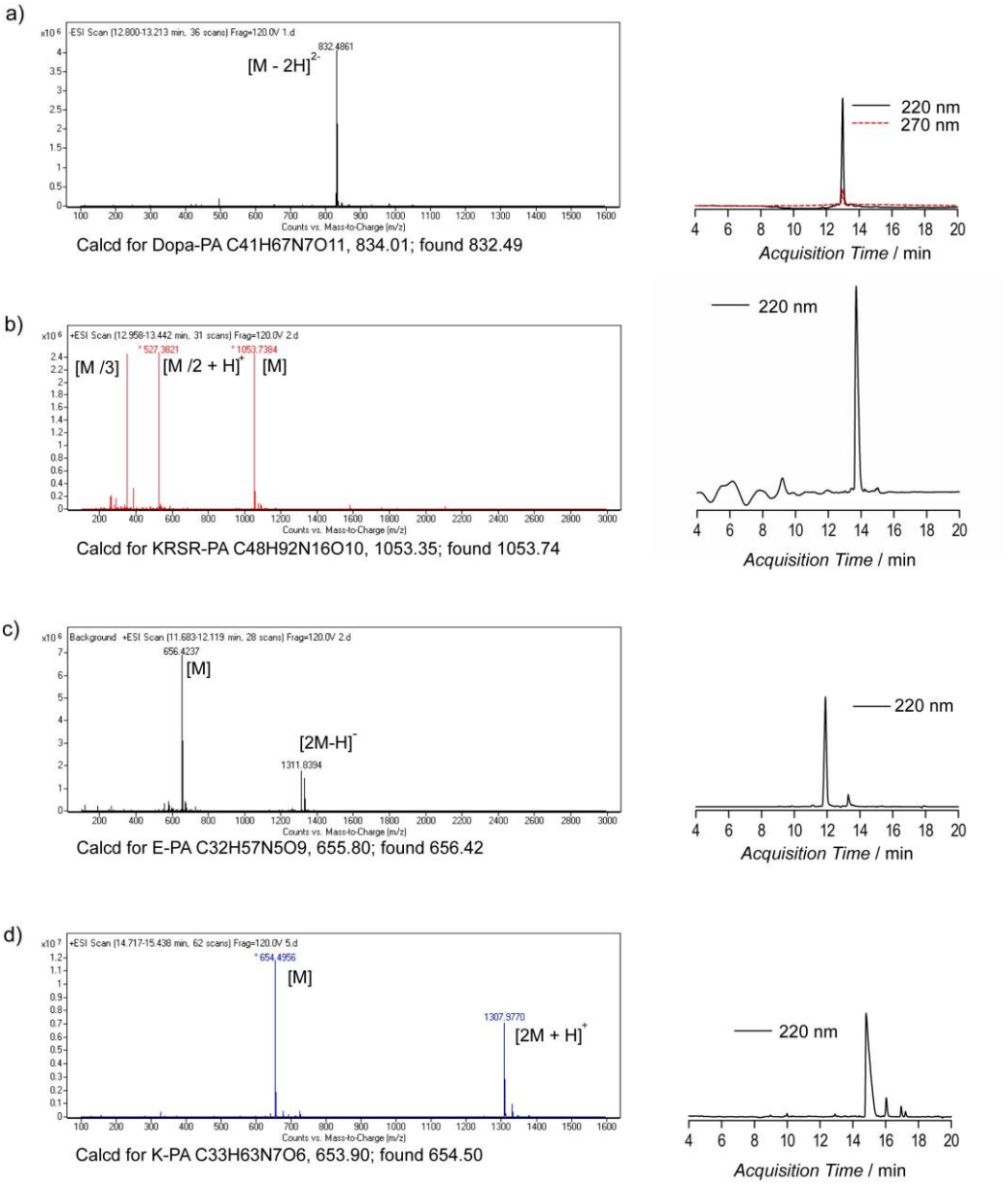

Figure 3.2 Mass spectra and liquid chromatograms of synthesized peptide amphiphiles. a) Dopa-PA, b) KRSR-PA, c) E-PA and d) K-PA.

It was seen that mixing two oppositely charged PA molecules brought the charge of the system up to zero at pH 7.4 (Figure 3.4 c).

3.3.4 Investigation of Surface Properties and Dopa-mediated Binding

Osteoconductive modification of titanium surface is crucial for successful integration of surrounding tissue in the long term. For this purpose, binding of KRSR-PA/Dopa-PA was investigated with XPS analysis in the presence of water. (Figure 3.5) We analyzed coated titanium surfaces after washing so that we could deduce the permanent absorption of KRSR-PA/Dopa-PA from complete suppression of photoelectron signal from the titanium substrate and the emergence of a strong nitrogen signal along with increased carbon signal. The results revealed that KRSR-PA/Dopa-PA nanofibers were coated on titanium surface successfully. To investigate the role of Dopa in surface adhesion mechanism, we tested KRSR-PA/E-PA nanofibers in the same way; however, these nanofibers were readily washed away from the surface in rinsing steps and hence did not form a permanent peptide layer according to the dramatically lowered nitrogen peak. Thus, we concluded that Dopa incorporation is critical for immobilization of peptide nanofibers on titanium surface. To further show the versatility of our system, we coated stainless steel and silicon wafer surfaces with KRSR-PA and Dopa-PA nanofibers. Similar results were also obtained for different surfaces. (Figure 3.6) To verify our conclusion from XPS results, we performed SEM imaging and FT-IR experiments. (Figure 3.7) SEM image of the KRSR-PA/Dopa-PA revealed that titanium surfaces were indeed coated with peptide nanofibers.

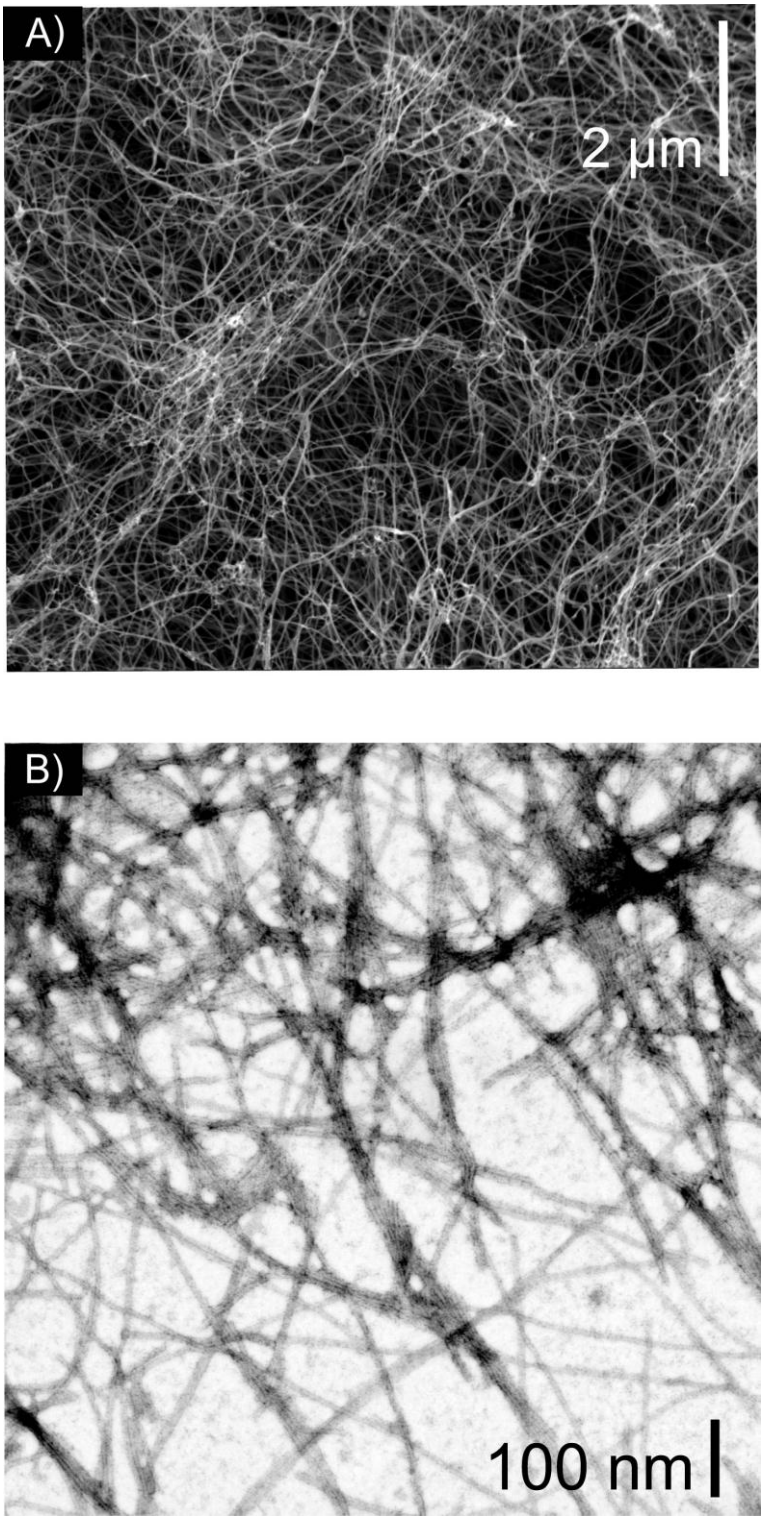

Figure 3.3 a) SEM, b) TEM images of the KRSR-PA/Dopa-PA nanofibers formed at pH 7.4

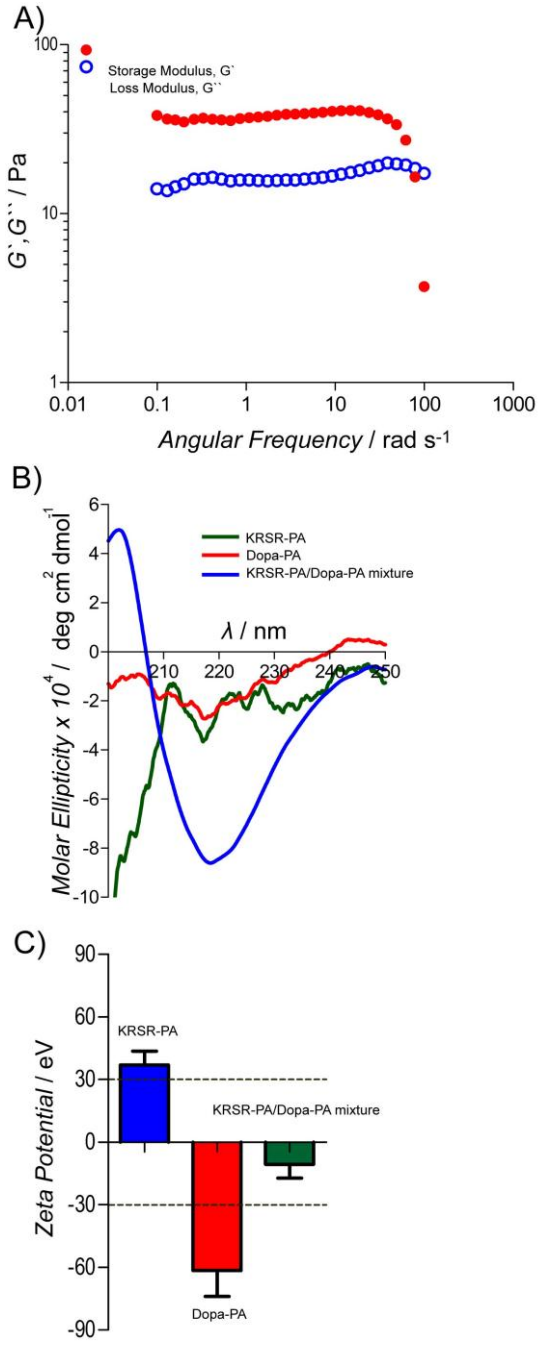

Figure 3.4 a) The mechanical properties of the KRSR-PA/Dopa-PA gel under varying angular frequencies. b) Circular dichroism and c) Zeta potential measurements of KRSR-PA, Dopa-PA, and their mixture, KRSR-PA/Dopa-PA.

Moreover, FT-IR spectra obtained from peptide nanofibers indicated the characteristic signals similar to previously reported Mefp-1 protein coating adsorbed on ZnSe surface which abundantly consisted of Dopa containing sequences in its protein structure. [136] Surface properties have an important role on determining cellular responses. It has been previously shown that osteoblasts and fibroblasts favor different surface characteristics depending on surface chemistry, hydrophilicity and topography as many other cells do. These parameters are highly important to determine the success of the implant. Since increased hydrophilicity and roughness are known to promote osteogenic activity, techniques such as titanium plasma spraying, oxide layer formation, acid etching, and electrochemical anodization were employed to roughen the surface and increase surface hydrophilicity.[137] In order to investigate surface hydrophilicity, we performed contact angle measurements on the peptide nanofibers. (Figure 3.8) Due to the nature of peptide amphiphiles, which hydrophilic ends were exposed to aqueous environment; they significantly contributed to hydrophilicity such that KRSR-PA/Dopa-PA showed more hydrophilic characteristics. Contact angle value of KRSR-PA/Dopa-PA coated surface decreased from 55.2º (bare titanium surface) to below 17º. For the same reason, a similar contact angle ($<17^{o}$) decrease was observed on K-PA/Dopa-PA nanofiber coated titanium surface (Figure S3C). To investigate the surface topography and coating homogeneity of KRSR-PA/Dopa-PA modified titanium surface, we measured roughness values of surfaces using optical profilometer (Figure 3.9).

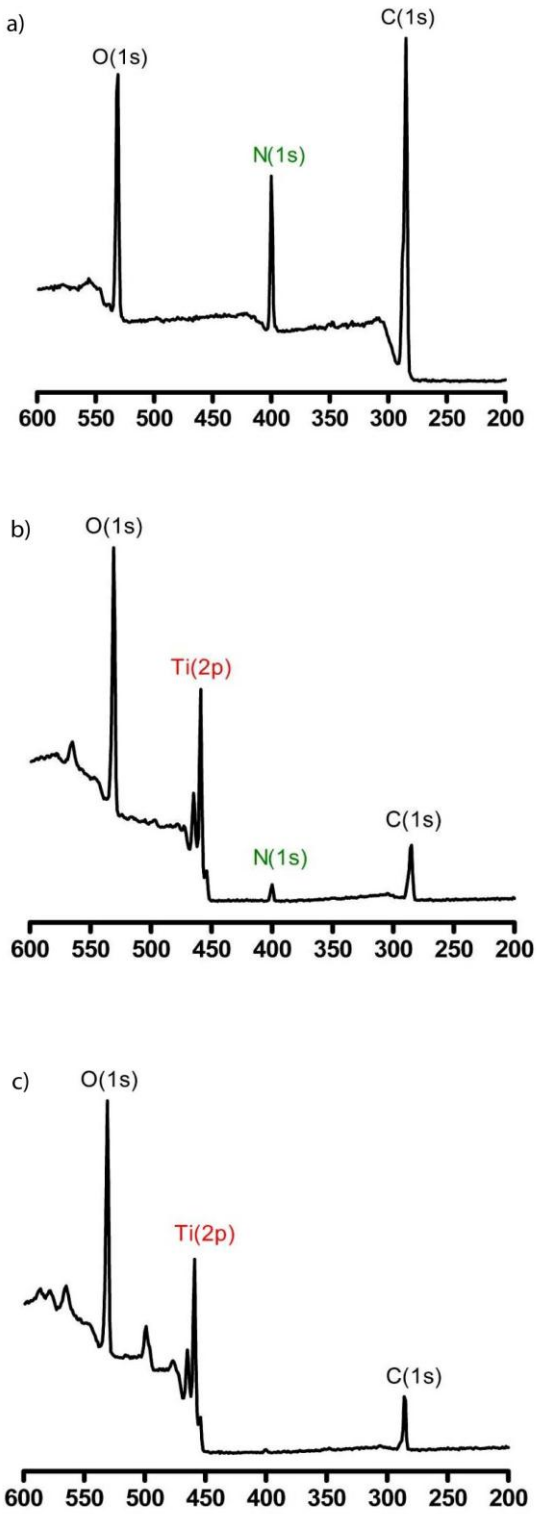

Figure 3.5 XPS spectra of a) KRSR-PA/Dopa-PA, b) KRSR-PA/E-PA coated titanium surfaces and c) bare titanium surface.

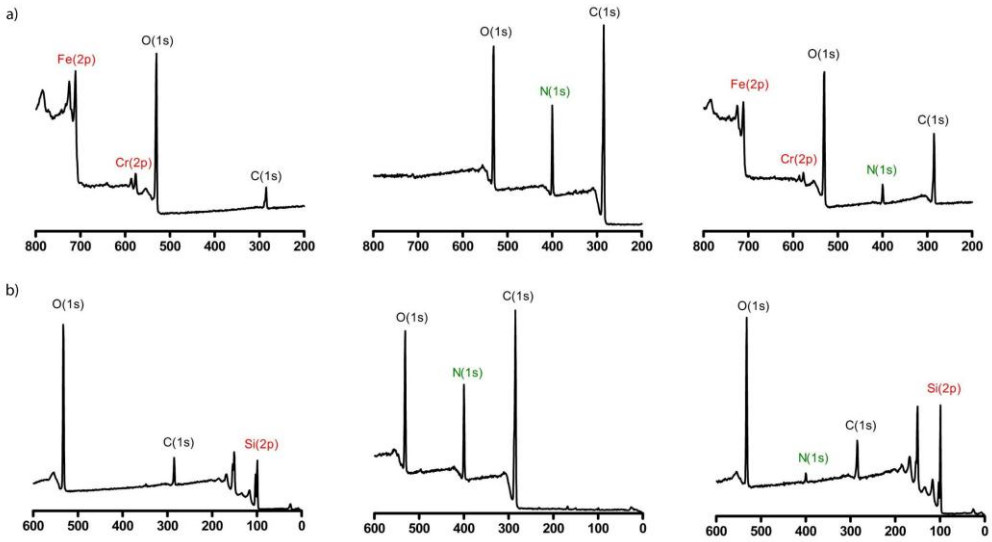

Figure 3.6 XPS spectra of functionalized a) stainless steel and b) silicon surfaces. Bare surface (left), KRSR-PA/Dopa-PA coated surface (middle) and KRSR-PA/E-PA coated surface (right).

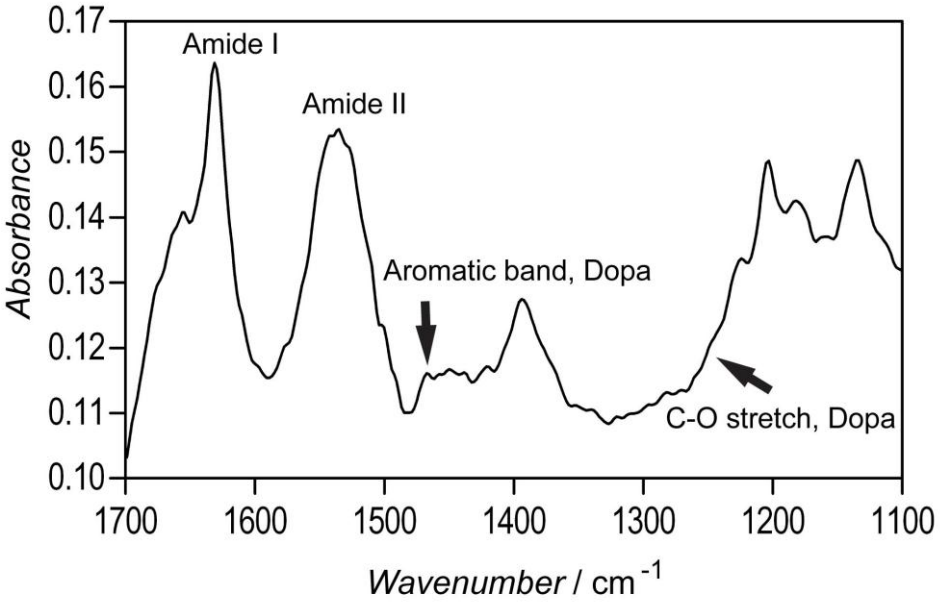

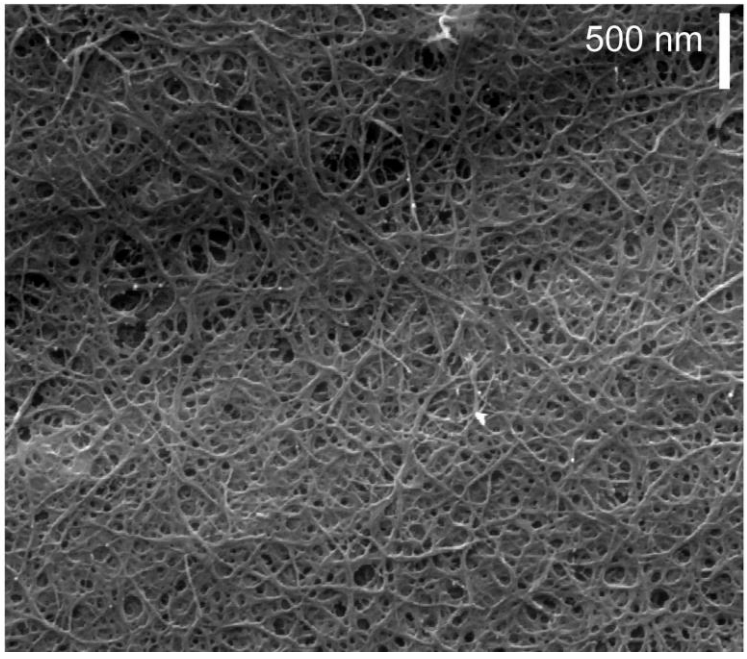

Figure 3.7 SEM micrograph of immobilized KRSR-PA/Dopa-PA nanofibers on titanium surface. (top) ATR/FT-IR spectrum of KRSR-PA/Dopa-PA nanofibers adhered on titanium surface. (bottom)

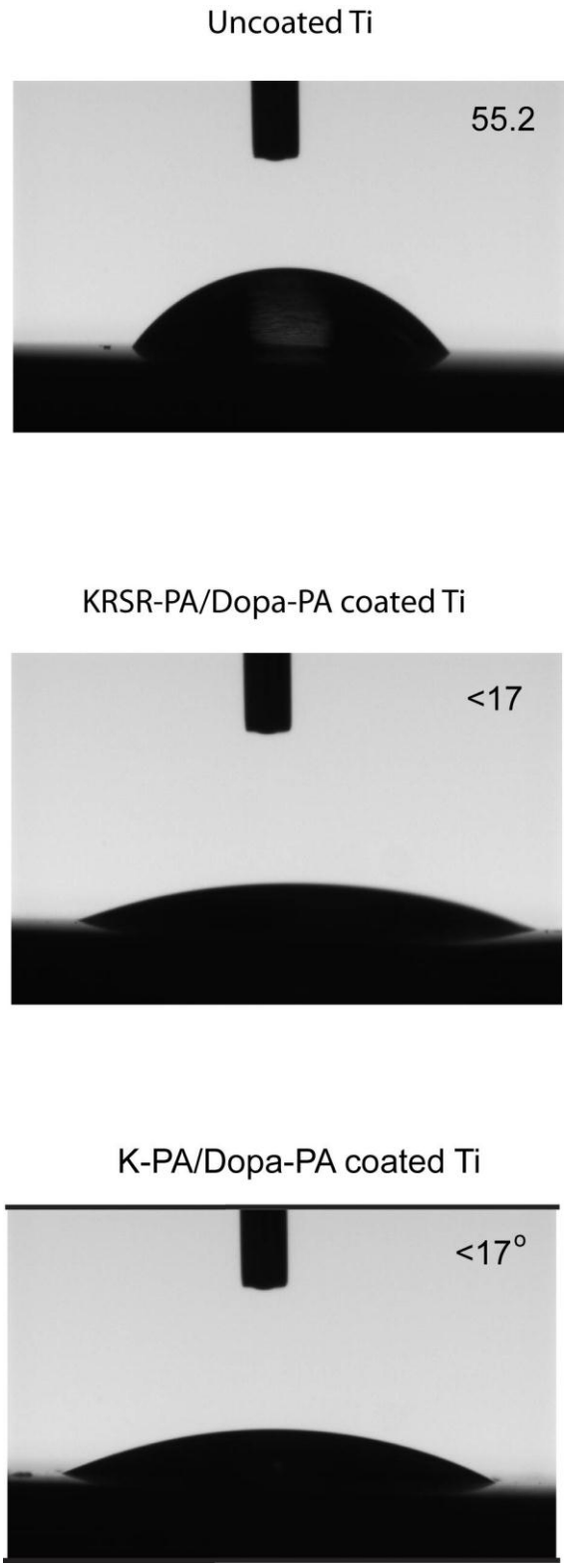

Figure 3.8 Contact angles of titanium substrates as bare (top), after KRSR-PA/Dopa-PA coating (middle) and after K-PA/Dopa-PA coating.

Surface roughness was found to increase on both KRSR-PA/Dopa-PA and K-PA/Dopa-PA coated titanium surfaces. To utilize the retention of the KRSR-PA/Dopa-PA nanofiber coating, we applied ultrasound sonication which is a powerful technique to break apart non-covalent molecular interactions and then investigated the contact angle change. (Figure 3.10) Contact angle of the surface after 1 h treatment increased to 33.1° from 55.2^{o}, indicating that despite detachment of some of the coating, a significant portion of the nanofibers still remained strongly bound to the surface. This relative increase can be ascribed to removal of the nanofibers that were not bound to the surface through Dopa-mediated titanium-catechol complexes; rather the nanofibers remained bound to the surface by physical entanglement of nanofibers. On the other hand, the remaining nanofibers attached to the surface through near-covalent strength of Dopa binding kept the contact angle below 55.2^{o}.

3.3.5 Effect of Surface-Adhesive and Osteogenic PAs on Cellular Behaviors

3.3.5.1 Cell Adhesion

Cell adhesion is mediated through interaction of cell surface proteins with ligands present in the proteins of the extracellular matrix. KRSR is one of the ligands found in the extracellular matrix, which binds to cell surface heparin and promote osteoblast adhesion. By culturing osteoblasts and fibroblasts in the absence of any adhesion proteins, and by preventing cells from synthesizing new adhesion proteins via cyclohexamide, we examined the role of KRSR on adhesion of osteoblasts and fibroblasts. We used K-PA as a control of KRSR-PA.

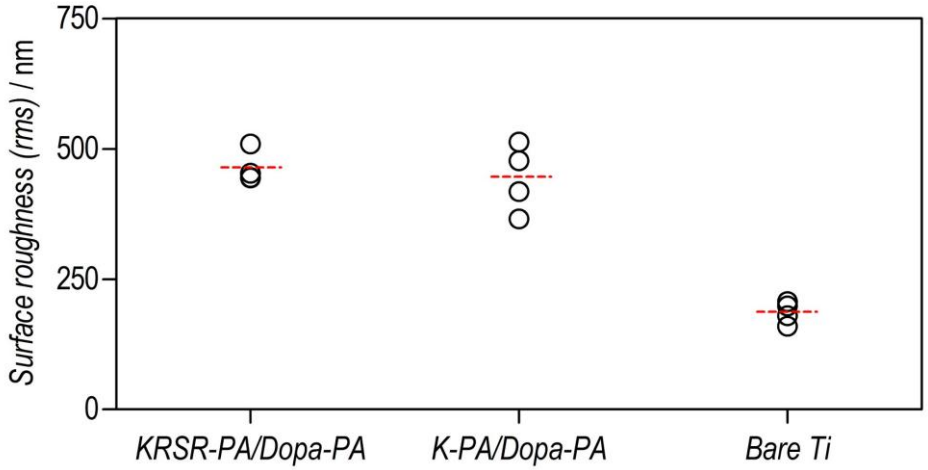

Figure 3.9 Roughness of KRSR-PA/Dopa-PA, K-PA/Dopa-PA coated and bare titanium surfaces.

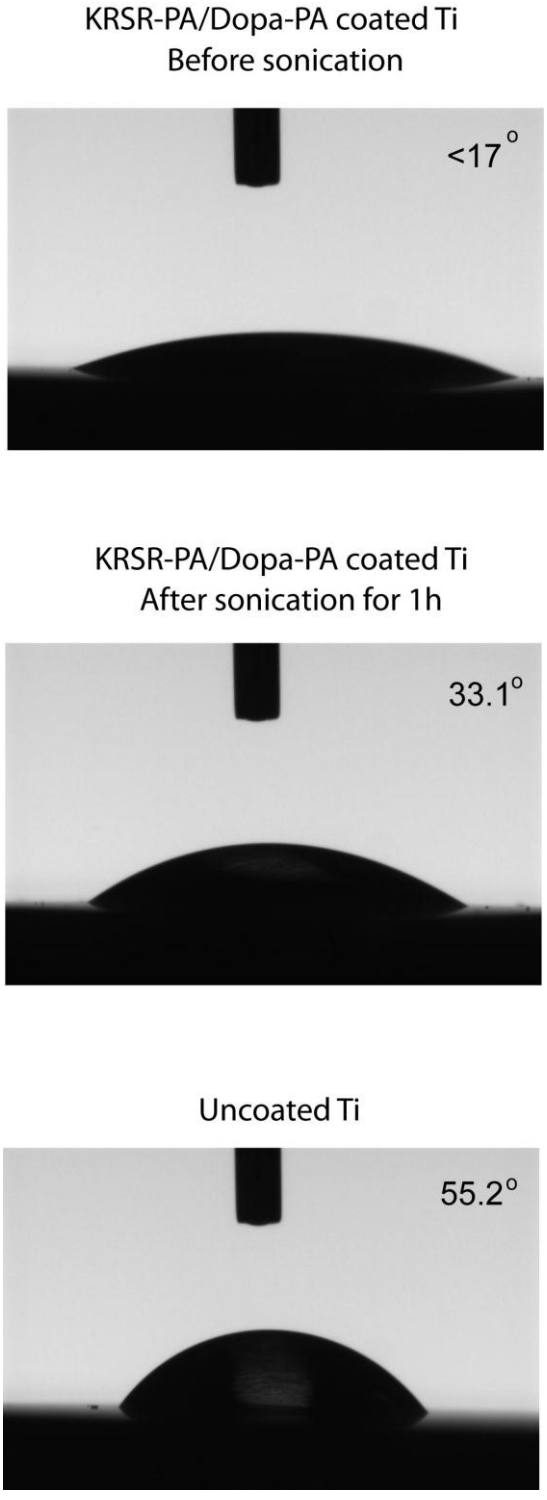

Figure 3.10 Contact angles of titanium substrates as bare, KRSR-PA/Dopa-PA coated and after 1 h sonication following KRSR-PA/Dopa-PA coating.

The number of osteoblastic Saos-2 cells adhered on KRSR-PA/Dopa-PA coated titanium surface at 1 h was 2.96 ± 0.19 folds greater than the cells adhered on bare titanium surface (Figure 3.11 a). We also observed that the number of Saos2 cells adhered on K-PA/Dopa-PA nanofibers was 2.51 ± 0.08 folds greater than the bare surface. We also noticed that the number of adhered Saos2 cells on KRSR-PA/Dopa-PA was significantly higher than K-PA/Dopa-PA, which indicates the role of KRSR in mediating osteoblast adhesion. To further investigate the bioactivity provided by peptide nanofibers, we analyzed adhesion behavior of MC3T3-E1 pre-osteoblast cells. The results were found to be in parallel to Saos2 adhesion, where cells adhered in significantly greater numbers on KRSR-PA/Dopa-PA compared to both K-PA/Dopa-PA and the bare surface. (Figure 3.11 a) We believed that the increased adhesion of osteoblasts and pre-osteoblasts on KRSR-lacking nanofibers compared to bare metal surface could be due to the altered surface properties upon peptide coating. It was previously reported that increased surface roughness and hydrophilicity promoted adhesion of osteoblasts. [138-139] On the other hand, the number of human gingival fibroblasts (HGF) adhered on KRSR-PA/Dopa-PA coated titanium surface decreased to 0.78 ± 0.06 fold of K-PA/Dopa-PA coated and 0.67 ± 0.05 fold of the bare titanium surface. (Figure 3.11 b) The significant difference between KRSR-PA/Dopa-PA and K-PA/Dopa-PA indicates the inhibitory role of KRSR toward fibroblast adhesion, because no other physical or chemical difference between these two nanofiber coatings was expected. Moreover, we observed that the fibroblast adhesion on K-PA/Dopa-PA decreased to 0.86 ± 0.06 fold of the

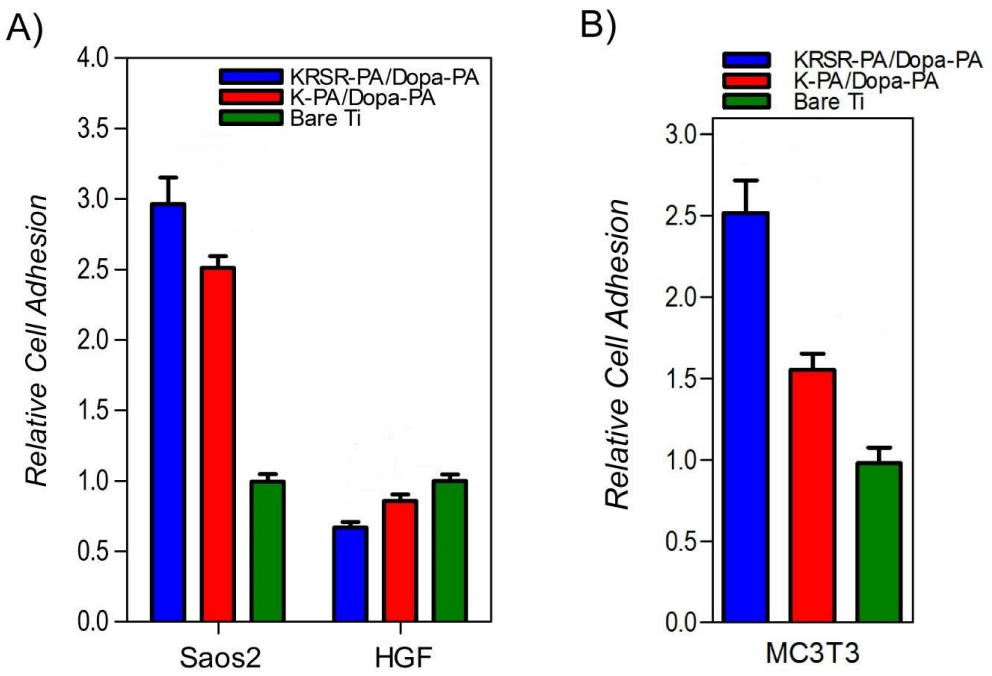

Figure 3.11 Adhesion of a) Saos-2, HGF and b) MC-3T3 cells on functionalized titanium surfaces.

bare surface. The reason could be that gingival fibroblasts favor hydrophobic and smoother surfaces, rather than rough and hydrophilic surfaces that osteoblasts do, which was also supported by previous findings.[140] Taken together, these results indicate that KRSR-PA/Dopa-PA nanofibers coated on titanium surfaces selectively favor osteoblast adhesion while inhibiting fibroblast adhesion.

3.3.5.2 Viability and Spreading

To see the effect of peptide nanofibers on cell viability, we incubated osteoblasts and fibroblasts on KRSR-PA/Dopa-PA for 24 h. We observed that viability of osteoblasts on KRSR-PA/Dopa-PA was significantly higher than other surfaces. (Figure 3.12 a) At the same time, viability of fibroblasts on KRSR-PA/Dopa-PA surfaces was significantly lower when compared to other surfaces. The number of viable osteoblasts on KRSR-PA/Dopa-PA coated titanium surface was 1.85 ± 0.19 folds greater compared to the cells on the bare surface and 1.17 ± 0.15 folds greater than K-PA/Dopa-PA coated surface. The viability of Saos-2 cells was also favored 1.58 ± 0.15 folds on K-PA/Dopa-PA with respect to bare titanium surface at 24 h. As in adhesion, KRSR ligand also has an important role in viability, however, it is less dominant when compared with other characteristics such as surface roughness and hydrophilicity when the difference between K-PA/Dopa-PA and bare titanium surface is taken into account. We found that the viability of MC3T3-E1 cells was comparable on all tested surfaces and there was not any significant difference between samples (Figure 3.12 c). In contrast, HGF viability dramatically decreased on PA coated surfaces. (Figure 3.12 b)

The viability of HGF decreased to almost 50% on KRSR-PA/Dopa-PA (0.55 ± 0.09 fold) and 75% on K-PA/Dopa-PA (0.75 ± 0.12 fold) compared to bare titanium surface. The viability of HGF cells decreased 0.73 ± 0.12 ($p<0.0001$) folds on KRSR-PA/Dopa-PA with respect to K-PA/Dopa-PA. From these results, we noticed that KRSR plays a strong inhibitory role on fibroblast viability. These cells attained round-like morphology on rougher and more hydrophilic PA coatings, which indicated an unfavorable microenvironment (Figure 3.13). Actin filament-stained HGFs further showed the loss of their characteristic elongated shapes on both KRSR-PA/Dopa-PA and K-PA/Dopa-PA coatings at 24 h (Figure 3.14). On the other hand, Saos2 cells attained their native morphology on PA coated surfaces before they do on bare titanium substrate. Considering cell adhesion, viability, and morphology of the cells, the KRSR-PA/Dopa-PA nanofibers provided a favorable microenvironment for osteoblast-like cells (Figure 3.13), while creating an inhibitory microenvironment for fibroblast cells.

3.3.5.3 ALP Activity & Mineralization

To see the effect of PA coated titanium surfaces on long term osteoblast adaptivity, we performed ALP activity and mineralization experiments. (Figure 3.15 a) ALP activity of Saos-2 cells on KRSR-PA/Dopa-PA and K-PA/Dopa-PA surfaces were significantly higher than ALP activity on bare surfaces throughout the course of experiments. ALP activity of cells was increased from day 1 to day 3 where maximum ALP activity was observed for all samples and

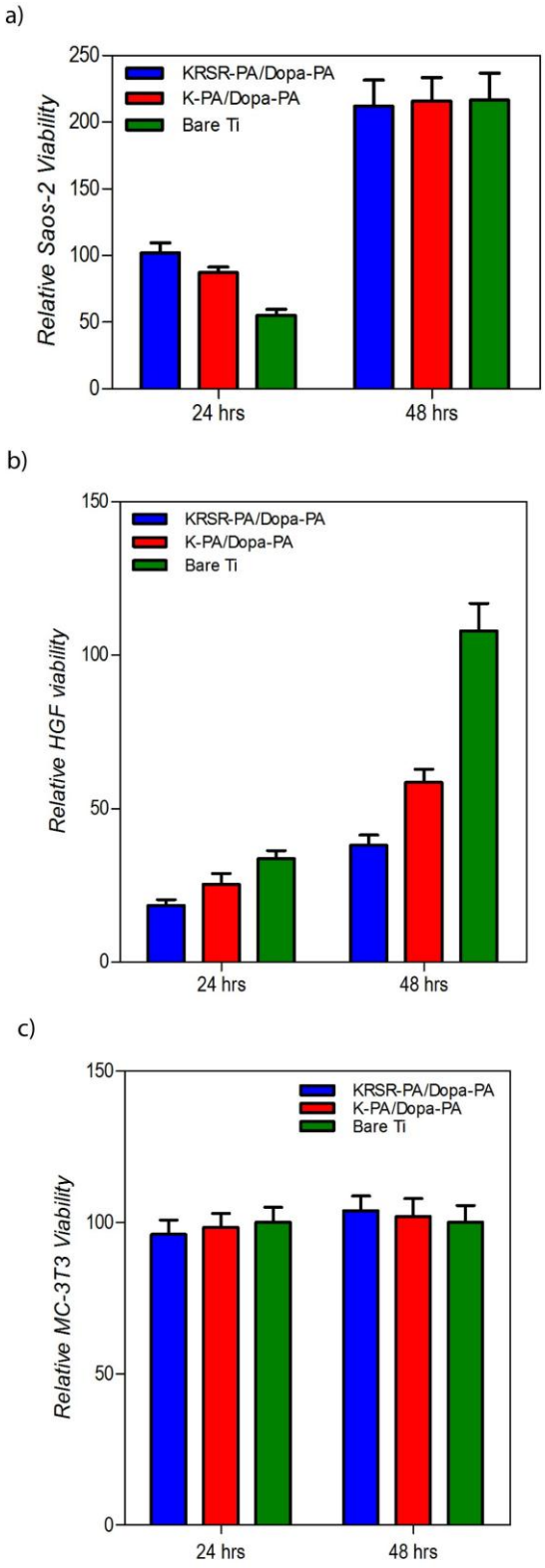

Figure 3.12 Viability of Saos-2, HGF and MC-3T3 cells after 24 h and 48 h of incubation.

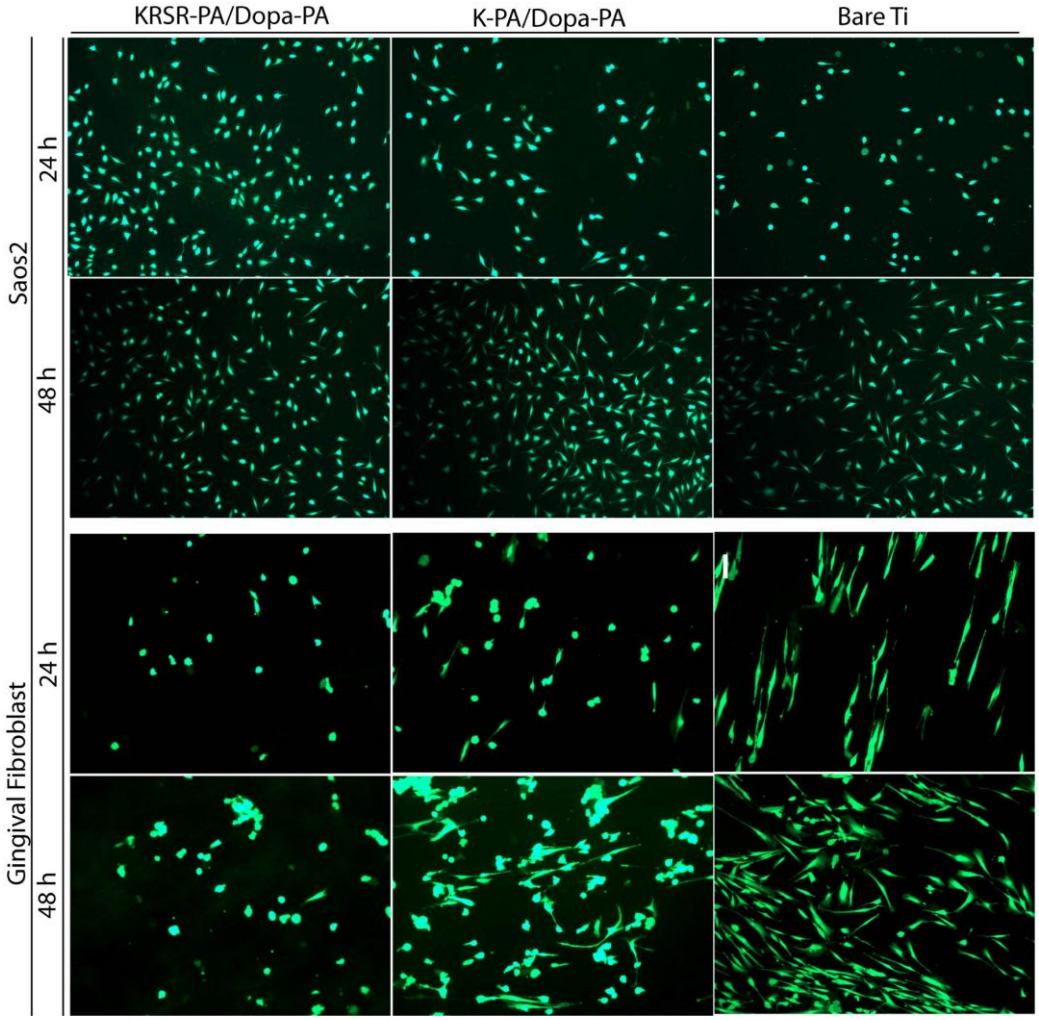

Figure 3.13 The morphology of osteoblasts and fibroblasts on functionalized titanium surfaces after 24 h and 48 h of incubation obtained by Calcein staining. (10x magnification)

ALP activity of cells was decreased after day 3 and remained constant from day 5 to day 7. ALP activity levels of cells on bare titanium surfaces remained low during the experiment. We didn't observe any significant difference between ALP activity of cells on KRSR-PA/Dopa-PA and K-PA/Dopa-PA surfaces on all days that we analyzed.

To test the effect of surfaces on calcium deposition of cells, we performed Alizarin Red staining after 14 and 21 days of incubation of cells in osteogenic medium. Because of the fact that titanium surfaces do not allow light transmission, we obtained macroscopic images of titanium surfaces by camera. We observed that staining of calcium deposits was higher on KRSR-PA/Dopa-PA and K-PA/Dopa-PA surfaces with respect to bare titanium surface. To quantify calcium deposition on titanium surfaces, we extracted Alizarin-Red bound calcium from surface via cetylpyridinium chloride through measuring absorbance at 562 nm. The results demonstrated significantly enhanced deposition of calcium-based minerals on KRSR-PA/Dopa-PA (1.34 ± 0.1 fold, $p < 0.05$) and K-PA/Dopa-PA (1.29 ± 0.09 fold, $p < 0.05$) coatings compared to bare titanium surface. (Figure 3.15 b and c) Similar mineral deposition pattern was also seen on day 21 for KRSR-PA/Dopa-PA (2.04 ± 0.15 fold) and K-PA/Dopa-PA (1.75 ± 0.18 fold) coatings compared to bare titanium surface. (Figure 3.15 c) When ALP activity and mineral deposition of cells on titanium surfaces were investigated, we observed similar patterns where KRSR-PA/Dopa-PA and K-PA/Dopa-PA surfaces showed higher ALP activity and mineral deposition compared to bare titanium surfaces.

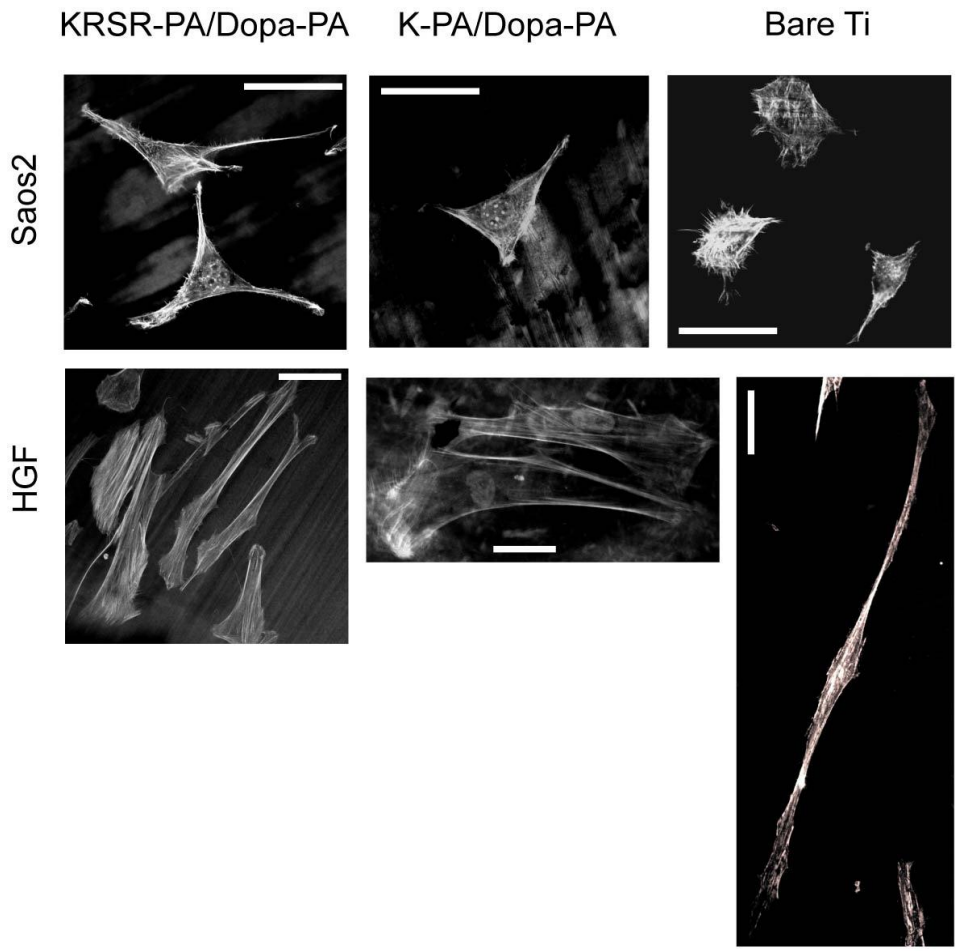

Figure 3.14 Representative high magnification confocal images of the cells at 24 h. Actin microfilaments and nuclei of cells were stained with TRITC-phalloidin and TO-PRO®, respectively. Scale bars show 50 μm.

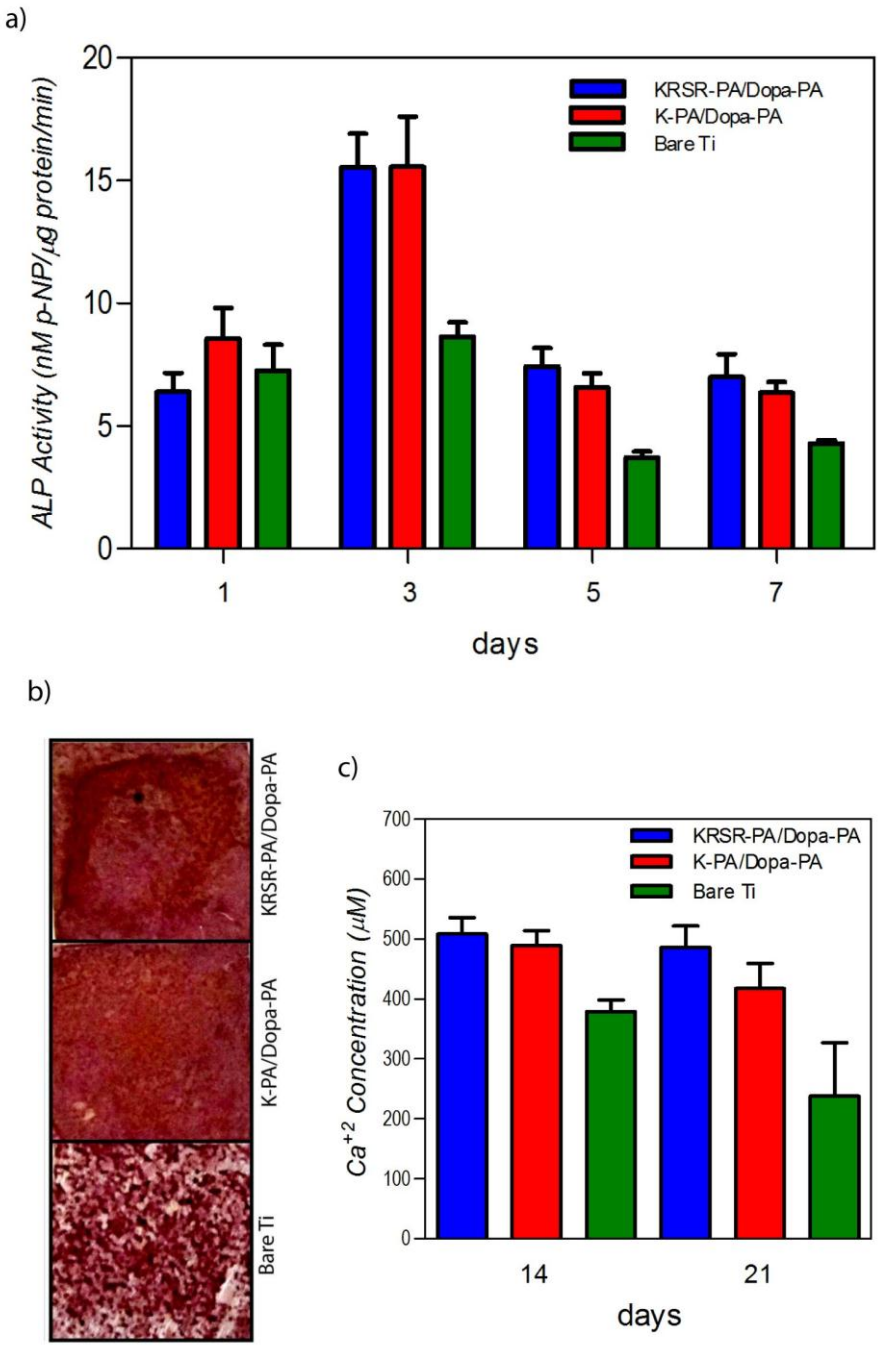

Figure 3.15 Mineralization experiments of osteoblasts on functionalized titanium surfaces. a) ALP activity of Saos-2 cells on day 1, 3, 5 and 7. b) Alizarin Red-S staining of calcium deposits on different surfaces. c) Calcium concentration of cells on functionalized titanium surfaces on day 14 and 21.

This indicates that ALP activity of cells, where inorganic phosphate pool is generated for calcium phosphate deposition in the early phase of the mineralization process, is correlated with the mineral deposition, which is a late marker of osteogenic activity. Moreover, we did not observe any differences between KRSR-PA/Dopa-PA and K-PA/Dopa-PA surfaces in terms of ALP activity and mineralization. The reason was that KRSR ligand affects the initial cellular responses such as adhesion and viability, however, when the long term activities of osteoblasts are taken into account, other factors like surface roughness and hydrophilicity could play a dominant role on the function of these cells.

3.4 Conclusion

Dopa-mediated immobilization of osteogenic peptide nanofibers on titanium surfaces created an osteoconductive interface between osteoblast-like cells and titanium substrate. The bottom-up surface engineering strategy presented in this work consisted of gathering ECM-derived osteoblast-specific peptide (KRSR) and mussel-inspired adhesive residue (Dopa) into ECM-mimetic peptide nanofibers under physiological conditions. This hybrid material was securely and homogenously immobilized onto titanium surface while maintaining its bioactive properties. XPS analysis after water treatment of coated surfaces and contact angle measurements performed following ultrasound sonication revealed that Dopa has an effective role on peptide nanofiber binding on surfaces. This binding is permanent and stronger with respect to peptide nanofibers where Dopa is not included. In addition, this bioactive surface coating selectively

favored osteoblast adhesion and growth while inhibiting adhesion and viability of soft tissue forming fibroblasts compared to uncoated titanium surface. Furthermore, ALP activity and mineralization experiments also indicated the success of bioactive titanium surfaces in the long term. For these reasons, this strategy can be extended to other surface immobilization systems due to the versatile adhesive properties of Dopa and the ease of ligand conjugation into peptide amphiphile molecules. By modifying the bioactive region of the peptide nanofiber system, a wide range of bioactive nanomaterials can be immobilized on various biomedical implants and devices. Overall, our strategy offers a general route for biofunctionalization of biomedical material surfaces using bottom-up fabricated self-assembled peptide nanofibers that can be functionalized in accordance with the application of interest.

Chapter 4

Conclusion and Future Perspectives

In order to develop a functional scaffold system to use in bone tissue engineering applications, a scaffold should be designed in a way that it has both osteoconductive and osteoinductive features and interacts with an appropriate cell source and growth factors. Self-assembled peptide nanofibers provide such an environment due to their versatile and functional structures. To achieve this, we developed two different nanofibrous network systems by self-assembly. In the first study, glycosaminoglycan-mimetic peptide nanofibers were designed to mimic the chemical groups on native glycosaminoglycans in the bone extracellular matrix, which have great importance in bone regeneration and mineralization process. These glycosaminoglycans can interact with various growth factors and also cell surface receptors to induce different osteogenic pathways via their functional groups. To mimic the structure of glycosaminoglycans, we decorated our peptide amphiphiles with carboxyl, hydroxyl and sulfonate groups that are abundant on the glycosaminoglycans found in bone. These functional groups triggered binding of BMP-2 on glycosaminoglycan-mimetic peptide nanofibers which provided osteoinductive characteristics to the peptide nanofibers. Cellular experiments revealed that, glycosaminoglycan-mimetic peptide nanofibers provided biocompatible and adapted microenvironment for osteoblastic cell growth, spreading and

proliferation. Moreover, osteogenic cells cultured on these nanofibers exhibited enhanced osteogenic activity. It was observed that alkaline phosphatase activity and calcium deposition which are the main indicators of bone-like mineralization were enhanced on these nanofibers. Furthermore, calcium phosphate mineralized collagen like fibrous structures were observed on these nanofibers with SEM. More importantly, osteogenic activity of cells was boosted in the presence of BMP-2 on sulfonated peptide nanofibers. As a result, this work indicates glycosaminoglycan-mimetic peptide nanofibers are osteoinductive materials which have potential for clinical applications of bone tissue engineering using either directly or as a carrier system together with growth factors. To achieve this, further experiments should be carried out with 3-D scaffold system in an *in vivo* model. This scaffold system could be successful by incorporating cells and bone related growth factors. Stem cells have great features such that they can give rise to different cell types including osteogenic cells and they can suppress immune reactions. Therefore, this type of combination could be closer to the perfect tissue engineering application. To test the effectiveness of glycosaminoglycan mimicking ability of peptide nanofibers, other studies such as changing sulfonation or carboxylation degree of peptide amphiphiles or their sequences could be studied and interaction with other bone related growth factors could be investigated.

In the second study, we developed a hybrid nanofiber system inspired by mussel adhesion mechanism. The nanofiber system was generated by mixing Dopa-conjugated peptide amphiphiles with osteogenic peptide amphiphiles which have

ECM-derived osteoblast-specific peptide (KRSR). An osteoconductive interface between osteoblast-like cells and the titanium substrate was created by Dopa-mediated immobilization of osteogenic peptide nanofibers on titanium surfaces. This hybrid material was securely and homogenously immobilized onto the titanium surface while maintaining its bioactive properties. XPS analysis after water treatment of coated surfaces and contact angle measurements performed following ultrasound sonication revealed that Dopa has an effective role on peptide nanofiber binding on surfaces. This binding was permanent and stronger with respect to peptide nanofibers where Dopa was not included. When other surfaces such as silica and stainless steel were coated with this hybrid material, similar results were obtained indicating the role of Dopa in adhesion. In addition, the bioactive surface coating selectively favored osteoblast adhesion and growth while inhibiting adhesion and viability of soft tissue forming fibroblasts compared to the uncoated titanium surface. This selective feature of the system is highly significant to prevent scar tissue formation and bone integration problems encountered in surgical interventions. Furthermore, ALP activity and mineralization experiments also indicated the success of bioactive titanium surfaces in the long term. For these reasons, this strategy can be extended to other surface immobilization systems due to the versatile adhesive properties of Dopa and the ease of ligand conjugation onto peptide amphiphile molecules. By modifying the bioactive region of the peptide nanofiber system, a wide range of bioactive nanomaterials can be immobilized on various biomedical implants and devices. As a result, our strategy offers a general route for biofunctionalization of

biomedical material surfaces using bottom-up fabricated self-assembled peptide nanofibers that can be functionalized in accordance with the application of interest. To indicate the future success of our strategy, *in vivo* models where biomedical implants (titanium implants, stents) coated with peptide nanofibers in this strategy should be performed. To further show the selectivity of this system for specific cell types (e.g. osteoblasts, endothelial cells) immunohistochemistry experiments could be performed using specific antibodies. Moreover, peptide sequences could be extended according to the complexity of target tissue. Finally, further experiments which test strength of Dopa-mediated binding should be carried out by considering flow pressure in the body.

Bibliography

1. Mehta, S.S., *Analysis of the Mechanical Properties of Bone Material Using Nondestructive Ultrasound Reflectometry*. 1995: University of Texas Southwestern Medical Center at Dallas.
2. Stevens, M.M., *Biomaterials for bone tissue engineering.* Materials Today, 2008. **11**(5): p. 18-25.
3. *The compressive behavior of bone as a two-phase porous structure.* The Journal of Bone & Joint Surgery, 1977. **59**(7): p. 954-962.
4. Weiner, S. and W. Traub, *Bone structure: from angstroms to microns.* FASEB J, 1992. **6**(3): p. 879-85.
5. Bullough, P.G., *The role of bone biopsy in evaluating bone disease.* Rev Rhum Engl Ed, 1997. **64**(6 Suppl): p. 37S-43S.
6. Marotti, G., *A new theory of bone lamellation.* Calcif Tissue Int, 1993. **53 Suppl 1**: p. S47-55; discussion S56.
7. Giraud-Guille, M., *Twisted plywood architecture of collagen fibrils in human compact bone osteons.* Calcified Tissue International, 1988. **42**(3): p. 167-180.
8. Reilly, D.T., A.H. Burstein, and V.H. Frankel, *The elastic modulus for bone.* J Biomech, 1974. **7**(3): p. 271-5.
9. Glimcher, M.J., *Mechanism of calcification: Role of collagen fibrils and collagen-phosphoprotein complexes in vitro and in vivo.* The Anatomical Record, 1989. **224**(2): p. 139-153.
10. Colfen, H., *Biomineralization: A crystal-clear view.* Nat Mater, 2010. **9**(12): p. 960-961.
11. Robey, P.G., et al., *Structure and molecular regulation of bone matrix proteins.* Journal of Bone and Mineral Research, 1993. **8**(S2): p. S483-S487.
12. Rho, J.Y., L. Kuhn-Spearing, and P. Zioupos, *Mechanical properties and the hierarchical structure of bone.* Med Eng Phys, 1998. **20**(2): p. 92-102.
13. Landis, W.J., *The strength of a calcified tissue depends in part on the molecular structure and organization of its constituent mineral crystals in their organic matrix.* Bone, 1995. **16**(5): p. 533-44.
14. Burg, K.J., S. Porter, and J.F. Kellam, *Biomaterial developments for bone tissue engineering.* Biomaterials, 2000. **21**(23): p. 2347-59.
15. Bauer, T.W. and G.F. Muschler, *Bone graft materials. An overview of the basic science.* Clin Orthop Relat Res, 2000(371): p. 10-27.
16. Boden, S.D., *Overview of the biology of lumbar spine fusion and principles for selecting a bone graft substitute.* Spine (Phila Pa 1976), 2002. **27**(16 Suppl 1): p. S26-31.
17. Stevens, M.M., et al., *In vivo engineering of organs: the bone bioreactor.* Proc Natl Acad Sci U S A, 2005. **102**(32): p. 11450-5.
18. Lord, C.F., et al., *Infection in bone allografts. Incidence, nature, and treatment.* J Bone Joint Surg Am, 1988. **70**(3): p. 369-76.

19. Netti, P.A., et al., *Hydrogels as an interface between bone and an implant.* Biomaterials, 1993. **14**(14): p. 1098-104.
20. Kretlow, J.D. and A.G. Mikos, *Review: mineralization of synthetic polymer scaffolds for bone tissue engineering.* Tissue Eng, 2007. **13**(5): p. 927-38.
21. Hench, L.L. and J.M. Polak, *Third-generation biomedical materials.* Science, 2002. **295**(5557): p. 1014-7.
22. Hartgerink, J.D., E. Beniash, and S.I. Stupp, *Peptide-amphiphile nanofibers: a versatile scaffold for the preparation of self-assembling materials.* Proc Natl Acad Sci U S A, 2002. **99**(8): p. 5133-8.
23. Hartgerink, J.D., E. Beniash, and S.I. Stupp, *Self-assembly and mineralization of peptide-amphiphile nanofibers.* Science, 2001. **294**(5547): p. 1684-8.
24. Wang, L. and J.P. Stegemann, *Thermogelling chitosan and collagen composite hydrogels initiated with beta-glycerophosphate for bone tissue engineering.* Biomaterials, 2010. **31**(14): p. 3976-85.
25. Cen, L., et al., *Collagen tissue engineering: development of novel biomaterials and applications.* Pediatr Res, 2008. **63**(5): p. 492-6.
26. Liao, S.S., et al., *Hierarchically biomimetic bone scaffold materials: nano-HA/collagen/PLA composite.* J Biomed Mater Res B Appl Biomater, 2004. **69**(2): p. 158-65.
27. Swetha, M., et al., *Biocomposites containing natural polymers and hydroxyapatite for bone tissue engineering.* Int J Biol Macromol, 2010. **47**(1): p. 1-4.
28. Lin, Y.C., et al., *Synthesis and characterization of collagen/hyaluronan/chitosan composite sponges for potential biomedical applications.* Acta Biomater, 2009. **5**(7): p. 2591-600.
29. Zou, C., et al., *Preparation and characterization of porous beta-tricalcium phosphate/collagen composites with an integrated structure.* Biomaterials, 2005. **26**(26): p. 5276-84.
30. Saffarzadeh, A., et al., *Comparison of two bone substitute biomaterials consisting of a mixture of fibrin sealant (Tisseel) and MBCP (TricOs) with an autograft in sinus lift surgery in sheep.* Clin Oral Implants Res, 2009. **20**(10): p. 1133-9.
31. Le Nihouannen, D., et al., *Micro-architecture of calcium phosphate granules and fibrin glue composites for bone tissue engineering.* Biomaterials, 2006. **27**(13): p. 2716-22.
32. Leeuwenburgh, S.C.G., et al., *Mineralization, Biodegradation, and Drug Release Behavior of Gelatin/Apatite Composite Microspheres for Bone Regeneration.* Biomacromolecules, 2010. **11**(10): p. 2653-2659.
33. Kim, I.Y., et al., *Chitosan and its derivatives for tissue engineering applications.* Biotechnol Adv, 2008. **26**(1): p. 1-21.
34. Zhang, Y. and M. Zhang, *Synthesis and characterization of macroporous chitosan/calcium phosphate composite scaffolds for tissue engineering.* J Biomed Mater Res, 2001. **55**(3): p. 304-12.

35. Kawakami, T., et al., *Experimental study on osteoconductive properties of a chitosan-bonded hydroxyapatite self-hardening paste.* Biomaterials, 1992. **13**(11): p. 759-63.
36. Di Martino, A., M. Sittinger, and M.V. Risbud, *Chitosan: A versatile biopolymer for orthopaedic tissue-engineering.* Biomaterials, 2005. **26**(30): p. 5983-5990.
37. Liu, X. and P.X. Ma, *Polymeric scaffolds for bone tissue engineering.* Ann Biomed Eng, 2004. **32**(3): p. 477-86.
38. Ma, P.X. and J.W. Choi, *Biodegradable polymer scaffolds with well-defined interconnected spherical pore network.* Tissue Eng, 2001. **7**(1): p. 23-33.
39. Zhao, F., et al., *Preparation and histological evaluation of biomimetic three-dimensional hydroxyapatite/chitosan-gelatin network composite scaffolds.* Biomaterials, 2002. **23**(15): p. 3227-34.
40. Kim, B.S. and D.J. Mooney, *Development of biocompatible synthetic extracellular matrices for tissue engineering.* Trends Biotechnol, 1998. **16**(5): p. 224-30.
41. Tessmar, J.K. and A.M. Gopferich, *Customized PEG-derived copolymers for tissue-engineering applications.* Macromol Biosci, 2007. **7**(1): p. 23-39.
42. Tan, H., et al., *Novel multiarm PEG-based hydrogels for tissue engineering.* Journal of Biomedical Materials Research Part A, 2010. **92A**(3): p. 979-987.
43. Fedorovich, N.E., et al., *Hydrogels as extracellular matrices for skeletal tissue engineering: state-of-the-art and novel application in organ printing.* Tissue Eng, 2007. **13**(8): p. 1905-25.
44. Sarvestani, A.S., X. He, and E. Jabbari, *Effect of osteonectin-derived peptide on the viscoelasticity of hydrogel/apatite nanocomposite scaffolds.* Biopolymers, 2007. **85**(4): p. 370-8.
45. Song, J., et al., *Elastomeric high-mineral content hydrogel-hydroxyapatite composites for orthopedic applications.* J Biomed Mater Res A, 2009. **89**(4): p. 1098-107.
46. Mujumdar, S.K. and R.A. Siegel, *Introduction of pH-Sensitivity into Mechanically Strong Nanoclay Composite Hydrogels Based on N-Isopropylacrylamide.* J Polym Sci A Polym Chem, 2008. **46**(19): p. 6630-6640.
47. Shu, X.Z., et al., *Synthesis and evaluation of injectable, in situ crosslinkable synthetic extracellular matrices for tissue engineering.* J Biomed Mater Res A, 2006. **79**(4): p. 902-12.
48. Garbern, J.C., A.S. Hoffman, and P.S. Stayton, *Injectable pH- and Temperature-Responsive Poly(N-isopropylacrylamide-co-propylacrylic acid) Copolymers for Delivery of Angiogenic Growth Factors.* Biomacromolecules, 2010. **11**(7): p. 1833-1839.
49. Tan, R., et al., *Preparation and characterization of an injectable composite.* J Mater Sci Mater Med, 2009. **20**(6): p. 1245-53.

50. Yan, C., et al., *Injectable solid hydrogel: mechanism of shear-thinning and immediate recovery of injectable beta-hairpin peptide hydrogels.* Soft Matter, 2010. **6**(20): p. 5143-5156.
51. Spoerke, E.D., S.G. Anthony, and S.I. Stupp, *Enzyme Directed Templating of Artificial Bone Mineral.* Adv Mater, 2009. **21**(4): p. 425-430.
52. Mata, A., et al., *Bone regeneration mediated by biomimetic mineralization of a nanofiber matrix.* Biomaterials, 2010. **31**(23): p. 6004-12.
53. Beniash, E., et al., *Self-assembling peptide amphiphile nanofiber matrices for cell entrapment.* Acta Biomater, 2005. **1**(4): p. 387-97.
54. Balasundaram, G. and T.J. Webster, *Increased osteoblast adhesion on nanograined Ti modified with KRSR.* J Biomed Mater Res A, 2007. **80**(3): p. 602-11.
55. Harbers, G.M. and K.E. Healy, *The effect of ligand type and density on osteoblast adhesion, proliferation, and matrix mineralization.* J Biomed Mater Res A, 2005. **75**(4): p. 855-69.
56. Huang, Z., et al., *Bioactive nanofibers instruct cells to proliferate and differentiate during enamel regeneration.* J Bone Miner Res, 2008. **23**(12): p. 1995-2006.
57. Yoshii, T., et al., *Fresh bone marrow introduction into porous scaffolds using a simple low-pressure loading method for effective osteogenesis in a rabbit model.* Journal of Orthopaedic Research, 2009. **27**(1): p. 1-7.
58. Lane, J.M., et al., *Metabolic bone disease and Paget's disease in the elderly. Part I: Metabolic bone disease.* Clin Rheum Dis, 1986. **12**(1): p. 49-70.
59. Mauney, J.R., V. Volloch, and D.L. Kaplan, *Role of adult mesenchymal stem cells in bone tissue engineering applications: current status and future prospects.* Tissue Eng, 2005. **11**(5-6): p. 787-802.
60. Noshi, T., et al., *Enhancement of the in vivo osteogenic potential of marrow/hydroxyapatite composites by bovine bone morphogenetic protein.* Journal of Biomedical Materials Research, 2000. **52**(4): p. 621-630.
61. Lattanzi, W., et al., *Ex vivo-transduced autologous skin fibroblasts expressing human Lim mineralization protein-3 efficiently form new bone in animal models.* Gene Ther, 2008. **15**(19): p. 1330-43.
62. Phillips, J.E., R.E. Guldberg, and A.J. Garcia, *Dermal fibroblasts genetically modified to express Runx2/Cbfa1 as a mineralizing cell source for bone tissue engineering.* Tissue Eng, 2007. **13**(8): p. 2029-40.
63. Tsuda, H., et al., *Efficient BMP2 gene transfer and bone formation of mesenchymal stem cells by a fiber-mutant adenoviral vector.* Mol Ther, 2003. **7**(3): p. 354-65.
64. Bostrom, M.P., et al., *Immunolocalization and expression of bone morphogenetic proteins 2 and 4 in fracture healing.* J Orthop Res, 1995. **13**(3): p. 357-67.

65. Ripamonti, U. and N. Duneas, *Tissue Morphogenesis and Regeneration by Bone Morphogenetic Proteins.* Plastic and Reconstructive Surgery, 1998. **101**(1): p. 227-239.
66. Johnson, E.E., M.R. Urist, and G.A. Finerman, *Repair of segmental defects of the tibia with cancellous bone grafts augmented with human bone morphogenetic protein. A preliminary report.* Clin Orthop Relat Res, 1988(236): p. 249-57.
67. Yasko, A.W., et al., *The healing of segmental bone defects, induced by recombinant human bone morphogenetic protein (rhBMP-2). A radiographic, histological, and biomechanical study in rats.* J Bone Joint Surg Am, 1992. **74**(5): p. 659-70.
68. Sampath, T.K., et al., *Recombinant human osteogenic protein-1 (hOP-1) induces new bone formation in vivo with a specific activity comparable with natural bovine osteogenic protein and stimulates osteoblast proliferation and differentiation in vitro.* J Biol Chem, 1992. **267**(28): p. 20352-62.
69. Wang, E.A., et al., *Recombinant human bone morphogenetic protein induces bone formation.* Proc Natl Acad Sci U S A, 1990. **87**(6): p. 2220-4.
70. Croteau, S., et al., *Bone morphogenetic proteins in orthopedics: from basic science to clinical practice.* Orthopedics, 1999. **22**(7): p. 686-95; quiz 696-7.
71. Lee, S.G., et al., *End-functionalized glycopolymers as mimetics of chondroitin sulfate proteoglycans.* Chem Sci, 2010. **1**(3): p. 322-325.
72. He, X., X. Yang, and E. Jabbari, *Combined Effect of Osteopontin and BMP-2 Derived Peptides Grafted to an Adhesive Hydrogel on Osteogenic and Vasculogenic Differentiation of Marrow Stromal Cells.* Langmuir, 2012. **28**(12): p. 5387-5397.
73. Pham, Q.P., et al., *The influence of an in vitro generated bone-like extracellular matrix on osteoblastic gene expression of marrow stromal cells.* Biomaterials, 2008. **29**(18): p. 2729-39.
74. Bi, Y., et al., *Extracellular matrix proteoglycans control the fate of bone marrow stromal cells.* J Biol Chem, 2005. **280**(34): p. 30481-9.
75. Rozario, T. and D.W. DeSimone, *The extracellular matrix in development and morphogenesis: a dynamic view.* Dev Biol, 2010. **341**(1): p. 126-40.
76. Robey, P.G., A.L. Boskey, and Asbmr, *Chapter 6. The Composition of Bone*, in *Primer on the Metabolic Bone Diseases and Disorders of Mineral Metabolism*. 2009, John Wiley & Sons, Inc. p. 32-38.
77. Taipale, J. and J. Keski-Oja, *Growth factors in the extracellular matrix.* FASEB J, 1997. **11**(1): p. 51-9.
78. Mathews, S., et al., *Glycosaminoglycans enhance osteoblast differentiation of bone marrow derived human mesenchymal stem cells.* Journal of Tissue Engineering and Regenerative Medicine, 2012: p. n/a-n/a.

79. Mania, V.M., et al., *A comparative biochemical analysis of glycosaminoglycans and proteoglycans in human orthotopic and heterotopic bone.* IUBMB Life, 2009. **61**(4): p. 447-52.
80. van der Harst, M.R., et al., *An integral biochemical analysis of the main constituents of articular cartilage, subchondral and trabecular bone.* Osteoarthritis Cartilage, 2004. **12**(9): p. 752-61.
81. Prince, C.W. and J.M. Navia, *Glycosaminoglycan alterations in rat bone due to growth and fluorosis.* J Nutr, 1983. **113**(8): p. 1576-82.
82. Wollenweber, M., et al., *Mimicked bioartificial matrix containing chondroitin sulphate on a textile scaffold of poly(3-hydroxybutyrate) alters the differentiation of adult human mesenchymal stem cells.* Tissue Eng, 2006. **12**(2): p. 345-59.
83. Miyazaki, T., et al., *Oversulfated chondroitin sulfate-E binds to BMP-4 and enhances osteoblast differentiation.* J Cell Physiol, 2008. **217**(3): p. 769-77.
84. Nagahata, M., et al., *A novel function of N-cadherin and Connexin43: marked enhancement of alkaline phosphatase activity in rat calvarial osteoblast exposed to sulfated hyaluronan.* Biochem Biophys Res Commun, 2004. **315**(3): p. 603-11.
85. Theoleyre, S., et al., *Characterization of osteoprotegerin binding to glycosaminoglycans by surface plasmon resonance: role in the interactions with receptor activator of nuclear factor kappaB ligand (RANKL) and RANK.* Biochem Biophys Res Commun, 2006. **347**(2): p. 460-7.
86. Lamoureux, F., et al., *Glycosaminoglycans as potential regulators of osteoprotegerin therapeutic activity in osteosarcoma.* Cancer Res, 2009. **69**(2): p. 526-36.
87. Rider, C.C., *Heparin/heparan sulphate binding in the TGF-beta cytokine superfamily.* Biochem Soc Trans, 2006. **34**(Pt 3): p. 458-60.
88. Shinmyouzu, K., et al., *Dermatan sulfate inhibits osteoclast formation by binding to receptor activator of NF-kappa B ligand.* Biochem Biophys Res Commun, 2007. **354**(2): p. 447-52.
89. Fromigue, O., P.J. Marie, and A. Lomri, *Bone morphogenetic protein-2 and transforming growth factor-beta2 interact to modulate human bone marrow stromal cell proliferation and differentiation.* J Cell Biochem, 1998. **68**(4): p. 411-26.
90. Lecanda, F., L.V. Avioli, and S.L. Cheng, *Regulation of bone matrix protein expression and induction of differentiation of human osteoblasts and human bone marrow stromal cells by bone morphogenetic protein-2.* J Cell Biochem, 1997. **67**(3): p. 386-96.
91. Groeneveld, E.H. and E.H. Burger, *Bone morphogenetic proteins in human bone regeneration.* Eur J Endocrinol, 2000. **142**(1): p. 9-21.
92. Hollinger, J.O., et al., *Recombinant human bone morphogenetic protein-2 and collagen for bone regeneration.* J Biomed Mater Res, 1998. **43**(4): p. 356-64.

93. Ruppert, R., E. Hoffmann, and W. Sebald, *Human bone morphogenetic protein 2 contains a heparin-binding site which modifies its biological activity.* Eur J Biochem, 1996. **237**(1): p. 295-302.
94. Hynes, R.O., *The extracellular matrix: not just pretty fibrils.* Science, 2009. **326**(5957): p. 1216-9.
95. Kim, S.E., et al., *The effect of immobilization of heparin and bone morphogenic protein-2 (BMP-2) to titanium surfaces on inflammation and osteoblast function.* Biomaterials, 2011. **32**(2): p. 366-373.
96. Kang, Y., et al., *Creation of bony microenvironment with CaP and cell-derived ECM to enhance human bone-marrow MSC behavior and delivery of BMP-2.* Biomaterials, 2011. **32**(26): p. 6119-30.
97. Flynn, L.E., et al., *Proliferation and differentiation of adipose-derived stem cells on naturally derived scaffolds.* Biomaterials, 2008. **29**(12): p. 1862-71.
98. Bhrany, A.D., et al., *Development of an esophagus acellular matrix tissue scaffold.* Tissue Eng, 2006. **12**(2): p. 319-30.
99. Niece, K.L., et al., *Self-assembly combining two bioactive peptide-amphiphile molecules into nanofibers by electrostatic attraction.* J Am Chem Soc, 2003. **125**(24): p. 7146-7.
100. Dombrowski, C., et al., *Heparan sulfate mediates the proliferation and differentiation of rat mesenchymal stem cells.* Stem Cells Dev, 2009. **18**(4): p. 661-70.
101. Nikitovic, D., et al., *Effects of glycosaminoglycans on cell proliferation of normal osteoblasts and human osteosarcoma cells depend on their type and fine chemical compositions.* Anticancer Res, 2005. **25**(4): p. 2851-6.
102. Addison, W.N., et al., *Pyrophosphate inhibits mineralization of osteoblast cultures by binding to mineral, up-regulating osteopontin, and inhibiting alkaline phosphatase activity.* J Biol Chem, 2007. **282**(21): p. 15872-83.
103. Quarles, L.D., et al., *Distinct proliferative and differentiated stages of murine MC3T3-E1 cells in culture: an in vitro model of osteoblast development.* J Bone Miner Res, 1992. **7**(6): p. 683-92.
104. Jiao, X., et al., *Heparan sulfate proteoglycans (HSPGs) modulate BMP2 osteogenic bioactivity in C2C12 cells.* J Biol Chem, 2007. **282**(2): p. 1080-6.
105. McGEE-RUSSELL, S.M., *HISTOCHEMICAL METHODS FOR CALCIUM.* Journal of Histochemistry & Cytochemistry, 1958. **6**(1): p. 22-42.
106. Fedde, K.N., *Human osteosarcoma cells spontaneously release matrix-vesicle-like structures with the capacity to mineralize.* Bone Miner, 1992. **17**(2): p. 145-51.
107. Buttery, L.D., et al., *Differentiation of osteoblasts and in vitro bone formation from murine embryonic stem cells.* Tissue Eng, 2001. **7**(1): p. 89-99.

108. Nefussi, J.R., et al., *Sequential expression of bone matrix proteins during rat calvaria osteoblast differentiation and bone nodule formation in vitro.* J Histochem Cytochem, 1997. **45**(4): p. 493-503.
109. Laing, P.G., A.B. Ferguson, Jr., and E.S. Hodge, *Tissue reaction in rabbit muscle exposed to metallic implants.* J Biomed Mater Res, 1967. **1**(1): p. 135-49.
110. Hayashi, K., et al., *Quantitative analysis of in vivo tissue responses to titanium-oxide- and hydroxyapatite-coated titanium alloy.* J Biomed Mater Res, 1991. **25**(4): p. 515-23.
111. Spoerke, E.D., et al., *A bioactive titanium foam scaffold for bone repair.* Acta Biomater, 2005. **1**(5): p. 523-33.
112. Spoerke, E.D. and S.I. Stupp, *Synthesis of a poly(L-lysine)-calcium phosphate hybrid on titanium surfaces for enhanced bioactivity.* Biomaterials, 2005. **26**(25): p. 5120-9.
113. Hayashi, K., et al., *Effect of surface roughness of hydroxyapatite-coated titanium on the bone-implant interface shear strength.* Biomaterials, 1994. **15**(14): p. 1187-91.
114. Lavenus, S., G. Louarn, and P. Layrolle, *Nanotechnology and dental implants.* Int J Biomater, 2010. **2010**: p. 915327.
115. Wu, Y., et al., *Differential response of Staphylococci and osteoblasts to varying titanium surface roughness.* Biomaterials, 2011. **32**(4): p. 951-60.
116. Schliephake, H., et al., *Functionalization of dental implant surfaces using adhesion molecules.* J Biomed Mater Res B Appl Biomater, 2005. **73**(1): p. 88-96.
117. Morra, M., *Biochemical modification of titanium surfaces: peptides and ECM proteins.* Eur Cell Mater, 2006. **12**: p. 1-15.
118. Sargeant, T.D., et al., *Hybrid bone implants: self-assembly of peptide amphiphile nanofibers within porous titanium.* Biomaterials, 2008. **29**(2): p. 161-71.
119. Sargeant, T.D., et al., *Covalent functionalization of NiTi surfaces with bioactive peptide amphiphile nanofibers.* Biomaterials, 2008. **29**(8): p. 1085-98.
120. Petrie, T.A., et al., *Multivalent integrin-specific ligands enhance tissue healing and biomaterial integration.* Sci Transl Med, 2010. **2**(45): p. 45ra60.
121. Silva, G.A., et al., *Selective Differentiation of Neural Progenitor Cells by High-Epitope Density Nanofibers.* Science, 2004. **303**(5662): p. 1352-1355.
122. Dvir, T., et al., *Nanotechnological strategies for engineering complex tissues.* Nat Nanotechnol, 2011. **6**(1): p. 13-22.
123. Kraai, T., et al., *Complications of bone-anchored hearing aids in pediatric patients.* Int J Pediatr Otorhinolaryngol, 2011. **75**(6): p. 749-53.
124. Vale, F.M., et al., *Acrylic bone cement induces the production of free radicals by cultured human fibroblasts.* Biomaterials, 1997. **18**(16): p. 1133-5.

125. Pap, T., et al., *Osteoclast-independent bone resorption by fibroblast-like cells.* Arthritis Res Ther, 2003. **5**(3): p. R163-73.
126. Mostardi, R.A., et al., *In vitro response of human fibroblasts to commercially pure titanium.* J Biomed Mater Res, 1999. **47**(1): p. 60-4.
127. Dee, K.C., T.T. Andersen, and R. Bizios, *Design and function of novel osteoblast-adhesive peptides for chemical modification of biomaterials.* J Biomed Mater Res, 1998. **40**(3): p. 371-7.
128. Shin, H., S. Jo, and A.G. Mikos, *Biomimetic materials for tissue engineering.* Biomaterials, 2003. **24**(24): p. 4353-64.
129. Lee, H., J. Rho, and P.B. Messersmith, *Facile Conjugation of Biomolecules onto Surfaces via Mussel Adhesive Protein Inspired Coatings.* Adv Mater, 2009. **21**(4): p. 431-434.
130. Martin, S.M., et al., *Enhancing the biological activity of immobilized osteopontin using a type-1 collagen affinity coating.* J Biomed Mater Res A, 2004. **70**(1): p. 10-9.
131. Xiao, S.J., et al., *Immobilization of the cell-adhesive peptide Arg-Gly-Asp-Cys (RGDC) on titanium surfaces by covalent chemical attachment.* J Mater Sci Mater Med, 1997. **8**(12): p. 867-72.
132. Lee, H., et al., *Mussel-inspired surface chemistry for multifunctional coatings.* Science, 2007. **318**(5849): p. 426-30.
133. Choi, B.H., et al., *Cell behavior on extracellular matrix mimic materials based on mussel adhesive protein fused with functional peptides.* Biomaterials, 2010. **31**(34): p. 8980-8.
134. Lee, H., N.F. Scherer, and P.B. Messersmith, *Single-molecule mechanics of mussel adhesion.* Proc Natl Acad Sci U S A, 2006. **103**(35): p. 12999-3003.
135. Hamming, L.M., et al., *Mimicking mussel adhesion to improve interfacial properties in composites.* Compos Sci Technol, 2008. **68**(9): p. 2042-2048.
136. Fant, C., et al., *Investigation of Adsorption and Cross-Linking of a Mussel Adhesive Protein Using Attenuated Total Internal Reflection Fourier Transform Infrared Spectroscopy (ATR-FTIR).* The Journal of Adhesion, 2010. **86**(1): p. 25-38.
137. Novaes, A.B., Jr., et al., *Influence of implant surfaces on osseointegration.* Braz Dent J, 2010. **21**(6): p. 471-81.
138. Price, R.L., et al., *Selective bone cell adhesion on formulations containing carbon nanofibers.* Biomaterials, 2003. **24**(11): p. 1877-87.
139. Elias, K.L., R.L. Price, and T.J. Webster, *Enhanced functions of osteoblasts on nanometer diameter carbon fibers.* Biomaterials, 2002. **23**(15): p. 3279-87.
140. Kunzler, T.P., et al., *Systematic study of osteoblast and fibroblast response to roughness by means of surface-morphology gradients.* Biomaterials, 2007. **28**(13): p. 2175-2182.
141. Zeldich, E., et al., *Enamel matrix derivative stimulates human gingival fibroblast proliferation via ERK.* J Dent Res, 2007. **86**(1): p. 41-6.